Gut Microbial Trimethylamine is Elevated in Alcohol-Associated Hepatitis and Contributes to Ethanol-Induced Liver Injury in Mice

Robert N. Helsley[1,2,7*], Tatsunori Miyata[3*], Anagha Kadam[1,2*], Venkateshwari Varadharajan[1,2], Naseer Sangwan[1,2], Emily C. Huang[3], Rakhee Banerjee[1,2], Amanda L. Brown[1,2], Kevin K. Fung[1,2], William J. Massey[1,2], Chase Neumann[1,2], Danny Orabi[1,2], Lucas J. Osborn[1,2], Rebecca C. Schugar[1,2], Megan R. McMullen[3], Annette Bellar[3], Kyle L. Poulsen[3], Adam Kim[3], Vai Pathak[6], Marko Mrdjen[1,2,3], James T. Anderson[1,2], Belinda Willard[1,2], Craig J. McClain[13], Mack Mitchell[12], Arthur J. McCullough[2,3], Svetlana Radaeva[11], Bruce Barton[10], Gyongyi Szabo[9], Srinivasan Dasarathy[2,3], Jose Carlos Garcia-Garcia[8], Daniel M. Rotroff[6], Daniela S. Allende[5], Zeneng Wang[1,2], Stanley L. Hazen[1,2,4], Laura E. Nagy[2,3], and J. Mark Brown[1,2#]

[1]Department of Cardiovascular and Metabolic Sciences, Lerner Research Institute of the Cleveland Clinic, Cleveland, OH, USA
[2]Center for Microbiome and Human Health, Lerner Research Institute, Cleveland Clinic, Cleveland, OH, USA
[3]Department of Inflammation and Immunity, Lerner Research Institute, Cleveland Clinic, Cleveland, OH, USA
[4]Department of Cardiovascular Medicine, Heart and Vascular and Thoracic Institute, Cleveland Clinic, Cleveland, OH, USA
[5]Department of Anatomical Pathology, Cleveland Clinic, Cleveland, OH, USA
[6]Department of Quantitative Health Sciences, Lerner Research Institute, Cleveland Clinic, Cleveland, OH, USA
[7]Department of Pediatrics, Division of Pediatric Gastroenterology, Hepatology, and Nutrition, College of Medicine, University of Kentucky, Lexington, Kentucky, USA.
[8]Life Sciences Transformative Platform Technologies, Procter & Gamble, Cincinnati, OH, USA
[9]Department of Medicine, Beth Israel Deaconess Medical Center and Harvard Medical School, Boston, MA, USA
[10]Department of Population and Quantitative Health Sciences, University of Massachusetts Medical School, Worcester, MA, USA
[11]National Institute on Alcohol Abuse and Alcoholism, Bethesda, MD, USA
[12]Department of Internal Medicine, University of Texas Southwestern Medical Center, Dallas, TX, USA
[13]Department of Medicine, University of Louisville, Louisville, KY, USA
[*]Authors contributed equally to this work

[#] = To whom correspondence should be addressed: Department of Cardiovascular and Metabolic Sciences, Cleveland Clinic, Cleveland, OH 44195, USA. Tel: 216-444-8340; Fax: 216-444-9404; E-mail: brownm5@ccf.org

Running Title: Choline TMA lyase inhibition improves ethanol-induced liver injury

AUTHOR CONTRIBUTIONS

R.N.H. and J.M.B. planned the project, designed experiments, analyzed data, and wrote the first draft of the manuscript; J.C.G-G., S.L.H., and L.E.N. helped design experiments and provided useful discussion directing collaborative aspects of the project; C.J.M., M.M., A.J.M., S.D., B.B., G.S., S.D., and L.E.N. helped in patient recruitment, human sample collection, or clinical study coordination. R.N.H., T.M., A.K., V.V., N.S., E.H., R.B., A.L.B., K.K.F., W.M., C.N., D.O., L.J.O., R.C.S., M.R.M., A.B., K.L.P., A.K., V.P., M.M., J.T.A., B.W., D.M.R., D.S.A., and Z.W. either conducted mouse experiments, performed biochemical workup of mouse and human tissues, analyzed data, or aided in manuscript preparation; All authors were involved in the editing of the final manuscript.

ABSTRACT

BACKGROUND: There is mounting evidence that microbes resident in the human intestine contribute to diverse alcohol-associated liver diseases (ALD) including the most deadly form known as alcohol-associated hepatitis (AH). However, mechanisms by which gut microbes synergize with excessive alcohol intake to promote liver injury are poorly understood. Furthermore, whether drugs that selectively target gut microbial metabolism can improve ALD has never been tested.

METHODS: We used liquid chromatography tandem mass spectrometry to quantify the levels of microbe and host choline co-metabolites in healthy controls and AH patients, finding elevated levels of the microbial metabolite trimethylamine (TMA) in AH. In subsequent studies, we treated mice with non-lethal bacterial choline TMA lyase (CutC/D) inhibitors to blunt gut microbe-dependent production of TMA in the context of chronic ethanol administration. Indices of liver injury were quantified by complementary RNA sequencing, biochemical, and histological approaches. In addition, we examined the impact of ethanol consumption and TMA lyase inhibition on gut microbiome structure via 16S rRNA sequencing.

RESULTS: We show the gut microbial choline metabolite trimethylamine (TMA) is elevated in AH patients and correlates with reduced hepatic expression of the TMA oxygenase flavin-containing monooxygenase 3 (FMO3). Provocatively, we find that small molecule inhibition of gut microbial CutC/D activity protects mice from ethanol-induced liver injury. CutC/D inhibitor-driven improvement in ethanol-induced liver injury is associated with distinct reorganization of the gut microbiome and host liver transcriptome.

CONCLUSIONS: The microbial metabolite TMA is elevated in patients with AH, and inhibition of TMA production from gut microbes can protect mice from ethanol-induced liver injury.

KEYWORDS: liver disease, microbiome, metabolism, nutrition

INTRODUCTION

Alcohol-associated liver disease (ALD) includes a spectrum of liver pathologies including steatosis, fibrosis, cirrhosis, and the most severe manifestation known as alcohol-associated hepatitis (AH). Shortly after diagnosis AH patients die at a staggering rate of 40-50%[1,2]. Despite many attempts, an effective therapy for this deadly disease has been elusive. Similar to other components of the spectrum of ALD, AH has consistently been linked to reorganization of the gut microbiome and dysregulation of microbe-host interactions[3-14]. It is well appreciated that chronic alcohol use can elicit structural alterations in the gut barrier, allowing either live bacteria themselves or microbe-associated molecule patterns (MAMPs), such as lipopolysaccharide (LPS), to enter the portal circulation where they can directly engage pattern recognition receptors (PRRs) such as Toll-like receptors (TLRs) or NOD-like receptors (NLRP3, NLRP6, etc.) to promote hepatic inflammation and tissue injury[15-20]. In addition to MAMP-PRR interactions, gut microbes can act as a collective endocrine organ, producing a vast array of small molecules, proteins, and lipid metabolites that can engage dedicated host receptor systems to also impact liver disease progression[21]. Collectively, these MAMP-PRR and microbial metabolite-host receptor interactions converge to promote ALD and many other diseases of uncontrolled inflammation[21, 22].

Although there is now clear evidence that microbe-host interactions play a key role in liver disease progression[3-22], ALD drug discovery to this point has focused primarily on targets encoded by the human genome. Our knowledge is rapidly expanding as to how microbes intersect with ALD progression, including cataloging microbial genomes. We also now understand the repertoire of MAMPs gut microbes harbor as well as the vast array of metabolites that they produce in both patients with ALD and animal models of ethanol-induced liver injury[3-22]. However, there are very few examples of where this information has been leveraged into safe

and effective therapeutic strategies. In general, the microbiome-targeted therapeutic field has primarily focused on either anti-, pre-, or pro-biotic approaches, yet these microbial community-restructuring approaches have resulted in very modest or non-significant effects in clinical studies of liver disease[23-26]. As an alternative microbiome-targeted approach, we and others have begun developing non-lethal selective small molecule inhibitors of bacterial enzymes with the intention of reducing levels of disease-associated microbial metabolites with mechanistic rationale for contribution to disease pathogenesis[27-31]. In fact, we have recently shown that small molecule inhibition of the gut microbial transformation of choline into trimethylamine (TMA), the initial and rate-limiting step in the generation of the cardiovascular disease (CVD)-associated metabolite trimethylamine N-oxide (TMAO), can significantly reduce disease burden in animal models of atherosclerosis, thrombosis, heart failure, and chronic kidney disease[27-30]. Although the gut microbial TMAO pathway has been studied mostly in the context of CVD[32-39], recent studies found that breath levels of the primary metabolite TMA and other related co-metabolites are elevated in patients with ALD[40,41]. These data showed promise, but whether the gut microbial TMAO pathway is causally related to ALD has never been explored. Hence, here we set out to understand how the gut microbial TMA/TMAO pathway may play a contributory role in ALD susceptibility and progression, and to test whether selective drugs that lower gut microbial production of TMA can be an effective therapeutic strategy. In an era when host genetics/genomics approaches dominate, this work reminds us that genes and metabolic products produced by gut bacteria play equally important roles in modulating disease susceptibility. Whereas pathways encoded by the host genome have long been pursued as drug targets, this work provides proof of concept that rationally designed drugs that target bacterial metabolism likely have untapped therapeutic potential in ALD and beyond.

RESULTS

Circulating Levels of the Gut Microbial Metabolite Trimethylamine (TMA) are Elevated in Alcohol-Associated Hepatitis (AH)

In a previous collaborative study, we reported that the highly volatile microbial metabolite TMA is elevated in exhaled breath of patients with AH[40], and related co-metabolites, such as trimethyllysine and carnitine, can serve as prognostic indicators of mortality in AH[41]. Given the extremely volatile nature of TMA, it is readily detectable in breath, but is challenging to accurately quantitate levels in the circulation because TMA rapidly dissipates during collection and storage. To reduce the volatility of TMA and enable its analysis in the circulation, we coordinated patient blood collection utilizing rapid acidification of separated plasma (protonated TMA has a lower vapor pressure) across a large multi-center AH consortium (Defeat Alcoholic Steatohepatitis – DASH consortium)[42,50,51]. This provided us the unique opportunity to accurately quantify circulating TMA levels in human subjects, including those with moderate or severe AH for the first time. Patient demographics and clinical characteristics for the cohort examined are summarized in Figure 1-table supplements 1-2. Importantly, MELD score, Maddrey's discriminant function score, Child-Pugh Score, aspartate aminotransferase (AST), total bilirubin, creatinine, and international normalized ratio (INR) were higher in patients with severe AH compared to moderate AH patients, while serum albumin was lower in severe AH compared to moderate AH patients. In agreement with previous breath metabolomics studies[40, 41], plasma TMA levels were significantly elevated in moderate and severe AH patients compared to healthy controls (Figure 1A). However, the CVD-related co-metabolite TMAO was reciprocally decreased in AH patients (Figure 1B). Given the reciprocal alterations in plasma TMA and TMAO levels, we next examined the expression of the host liver enzyme flavin-containing monooxygenase 3 (FMO3) which is the predominant TMA to TMAO converting enzyme in the adult liver[52]. Interestingly, mRNA levels for FMO3 are uniquely repressed in patients with more

severe AH (AH with liver failure (MELD 22-28) and AH with emergency liver transplant (MELD 18-21)), but not in other liver disease etiologies such as non-alcoholic fatty liver disease (NAFLD) or viral hepatitis (Figure 1C). In agreement with reduced mRNA levels (Figure 1C), patients with severe AH undergoing emergency liver transplant have marked reduction in FMO3 protein (Figure 1D), which likely contributes to elevations in plasma TMA (Figure 1A). Although ethanol feeding in mice does not consistently result in reduced hepatic *Fmo3* expression (data not shown), a single injection of lipopolysaccharide (LPS) to induce acute hepatic inflammation is associated with both a reduction in the expression of *Fmo3* and a significant increase in the TMA receptor trace amine-associated receptor 5 (*Taar5*) (Figure 1E). It is important to note that circulating levels of the key gut microbial substrates for TMA production (choline and carnitine) were not significantly altered in patients with AH compared to healthy controls (Figure 1-figure supplement 1). However, plasma levels of other TMA pathway co-metabolites (e.g. betaine and γ-butyrobetaine) were elevated in patients with AH compared to healthy controls (Figure 1-figure supplement 1). These findings, in addition to previous breath metabolomic studies[40, 41], provide evidence that TMA and related co-metabolites may allow for discrimination of AH from other liver diseases.

Microbial Choline TMA Lyase Inhibition Protects Mice from Ethanol-Induced Liver Injury

We next sought to establish whether a causal relationship between gut microbial TMA production and ALD progression exists, and to test the hypothesis that selectively drugging microbial choline → transformation can serve as a mechanism for improving host liver disease and attenuating ethanol-induced liver injury in mice. Mice were individually treated with two recently reported non-lethal bacterial choline TMA lyase inhibitors, IMC and FMC[27]. These small molecule inhibitors exhibit potent *in vivo* inhibition of the gut microbial choline TMA lyase enzyme

CutC[53], and have been shown to effectively block bacterial choline to TMA conversion in vivo[27]. Designed as suicide substrate mechanism-based inhibitors, past studies reveal the vast majority of IMC and FMC is retained in the gut within luminal bacteria and excreted in the feces with limited systemic exposure of the polar drug in the host[27,29,30].

IMC treatment effectively blunted ethanol-induced increases in plasma TMA and TMAO (Figure 2A and B). IMC also produced modest increases in plasma choline and betaine, while reducing plasma carnitine, particularly in pair-fed mice (Figure 2C-E). IMC also prevented ethanol-induced increases in alanine aminotransferase (ALT) and hepatic steatosis (Figure 2F,G, and K). Interestingly, IMC treatment prevented ethanol-induced increases in hepatic triglycerides (Figure 2G), and reduced hepatic total and cholesterol esters, but not free cholesterol, in both pair- and ethanol-fed conditions (Figure 2H-I). IMC treatment also reduced the expression levels of the pro-inflammatory cytokine tumor necrosis factor α (*Tnfα)* (Figure 2L). Although IMC was well tolerated in several previous mouse studies in the setting of standard rodent chow-feeding[27,29,30], here we found an unexpected reduction in food intake and body weights in mice receiving both IMC and ethanol (Figure 2-figure supplement 1). Although IMC was clearly protective against ethanol-induced liver injury, this potential drug-ethanol interaction prompted us to test another structurally distinct gut microbe-targeted choline TMA lyase inhibitor FMC[27] (Figure 3 and Figure 3-figure supplement 1).

Importantly, FMC was well tolerated and did not significantly alter liquid diet intake or body weights throughout the 25-day chronic ethanol feeding study (Figure 2-figure supplement 1). FMC treatment trended towards reducing plasma TMA (Figure 3A), and more dramatically suppressed plasma TMAO levels (Figure 3B). Unlike IMC, which also altered other co-metabolites such as choline, betaine, and carnitine (Figure 2B-2E), FMC did not significantly alter these TMA co-metabolites (Figure 3C-3E). More importantly, as with IMC (Figure 2F-K),

FMC treatment significantly protected against ethanol-induced ALT elevations (Figure 3F), hepatic steatosis (Figure 3G and 3K), and reduced total and esterified cholesterol levels without altering free cholesterol (Figure 3H-J). However, FMC trended to reduce but did not significantly alter *Tnf*α expression (Figure 3L). To determine whether these effects were generalizable in other models of ethanol-induced liver injury, we exposed control and FMC-treated mice to a 10-day chronic model in which mice were allowed free access to a 5% vol/vol (27% kcal) for 10 days (Figure 3-figure supplement 1). In this 5%-10 day ethanol feeding model FMC treatment did not significantly alter food intake, body weight, or blood ethanol levels, but was able to selectively suppress TMA and TMAO levels (Figure 3-figure supplement 1). FMC treatment in the 5%-10 day model significantly reduced plasma AST and ALT levels, and trended towards lowering liver triglycerides (Figure 3-figure supplement 1). However, in this short-term model there were no apparent differences in hepatic cytokine/chemokine gene expression with either ethanol exposure or FMC treatment (Figure 3-figure supplement 1 and data not shown). Collectively, these data demonstrate that gut microbe-targeted choline TMA lyase inhibition with two structurally distinct inhibitors (IMC or FMC) can generally protect mice against ethanol-induced liver injury.

Microbial Choline TMA Lyase Inhibitors Promote Remodeling of the Gut Microbiome and Host Liver Transcriptome in an Ethanol-Dependent Manner

One theoretical advantage of the selective microbe-targeted choline TMA lyase inhibitors, compared to antibiotic or MAMP-PRR-targeted therapies, is that they are anticipated to exert less selective pressure for development of drug resistance given their non-lethal nature. However, microbes that preferentially utilize choline as a carbon or nitrogen source might be anticipated to have reduced competitive advantage in the presence of the inhibitor. We therefore

next examined whether IMC or FMC treatment was associated with alterations in choline utilizers and other members of the murine gut microbiome community that are known to be correlated with ethanol-induced liver injury[3-14]. It is important to note that both IMC (Figure 4A-4E) and FMC (Figure 4F-4J) altered the gut microbiome, with some consistency yet several distinct differences. Non-metric multidimensional scaling (NMDS) of microbial taxa revealed distinct clusters, indicating that both IMC and FMC promoted clear restructuring of the cecal microbiome in an ethanol-dependent manner (Figure 4A and 4F). Under pair feeding conditions both IMC and FMC caused a reciprocal decrease in the relative abundance of *Bacteroidetes* and increase in *Firmicutes* (Figure 4B and 4G). However, under ethanol fed-conditions IMC resulted in increased *Bacteroidetes* and reduced *Firmicutes*, and FMC treatment resulted in more modest reductions in *Bacteroidetes* and increased *Firmicutes* (Figure 4B and 4G). When examining drug specific alterations at the genus level, we found that under both pair- and ethanol-fed conditions IMC treatment promoted significant increases in *Faecalibaculum* and *Escherichica/Shigella*, and reductions in *Bacteroidales_S24-7* (Figure 4C-E and 4H-I). FMC, however, most significantly altered *Turicibacter*, *Oscillibacter*, and *Lachnospiraceae*a, and it is important to note that these FMC-induced alterations were different between pair- and ethanol-fed groups (Figure 4C-E and 4H-I). Collectively, these data demonstrate that inhibition of gut microbial choline to TMA transformation with a selective non-lethal small molecule inhibitor promotes restructuring of the gut microbiome in an ethanol-dependent manner.

To more globally understand the effects of choline TMA lyase inhibitors on the host liver we performed unbiased RNA sequencing in mice undergoing pair- or ethanol-feeding treated either with or without IMC (Figure 5). NMDS and hierarchical clustering analysis showed clear separation between all four groups (Figure 5A and 5B). In pair-fed mice, IMC treatment caused significant decreases in several genes encoding major urinary proteins (*Mup2*, *Mup10*, *Mup11*,

and *Mup18*) and cytochrome p450 enzymes (*Cyp3a16*, *Cyp3a44*), while increasing other genes involved in xenobiotic metabolism (*Ephx1*, *Cyp4a31*) and hormone/cytokine signaling (*Lepr*, *Fgf21*, *Il22ra1*) (Figure 5C). Under ethanol-feeding conditions, IMC treatment most significantly altered genes involved in hepatocyte metabolism (*Cyp8b1*, *Ugt1a5*, *Pnpla5*, *Sult2a8, Ces3a*, and *Cmah*), RNA processing (*Ddx21*, *Ftsj3*, *Dus1l, and Cmah*), and again major urinary proteins (*Mup2*, *Mup10*, *Mup11*, and *Mup20*) (Figure 5D and 5E). These unbiased RNASeq data demonstrate that gut microbe-targeted choline TMA lyase inhibitors can alter the host liver transcriptome in an ethanol feeding-dependent manner.

The Microbe-Derived Metabolite TMA Elicits Rapid Hormone-Like Signaling Effects in Mouse Liver

The gut microbe-derived co-metabolites TMA and TMAO are generated postprandially in both rodents and humans after a substrate-rich meal is ingested[55-56]. Given the acute meal-related production and recent identification of candidate host receptors for TMA[57,58] and TMAO[59], we hypothesized that TMA may be acting as a gut microbe-derived hormone to promote liver injury. However, currently nothing is known regarding the acute hormone-like signaling effects stimulated by TMA in the liver. To address this gap, we infused TMA directly into the portal circulation draining the gut (i.e. portal vein) of fasted mice and examined global phosphorylation events stimulated in the liver ten minutes later using a phosphoproteomics approach. It is important to note that this experiment provided high levels of exogenous TMA via direct injection, and future studies should focus on more physiologically relevant modes of TMA production like provision of gut bacteria that can naturally or be genetically engineered to produce high levels. A total of 36 liver proteins exhibited site-specific hypo- or hyper-phosphorylation 10 minutes after administration of TMA relative to vehicle-injected mice (Figure 6B). Several of the TMA-driven

phosphorylation events represented proteins that are enriched in key hormonal signaling pathways known to impact hepatic metabolism. For example, portal vein infusion of TMA resulted in altered phosphorylation of proteins implicated in protein kinase A (PKA) signaling, including A kinase anchor protein 1 (AKAP1)[60] and FK506-binding protein 15 (FKBP15)[61], and insulin signaling including insulin receptor substrate 2 (IRS2)[62] (Figure 6B-6D). TMA infusion was also associated with altering the phosphorylation of several guanine nucleotide exchange factors (GEF) including Rac/Cdc42 guanine nucleotide exchange factor 6 (Arhgef6) and Rho GTPase activating protein 17 (ARHGAP17)[63,64], and proteins involved in RNA processing/splicing including signal recognition particle 14 (SRP14)[65] and serine and arginine rich splicing factor 1 (SRSF1)[66] (Figure 6B and 6C). These data have identified acute TMA-driven signaling events in the liver *in vivo*, and potentially link TMA to acute alterations in PKA-, insulin-, and GEF-driven signaling cascades that deserve further exploration.

DISCUSSION

Although drug discovery has historically targeted pathways in the human host, there is untapped potential in therapeutically targeting the gut microbial endocrine organ to treat advanced liver disease. This paradigm shift is needed in light of the clear and reproducible associations between the gut microbiome in viral, alcohol-associated, and non-alcohol associated liver diseases[3-21]. Now we are faced with both the challenge and opportunity to test whether microbe-targeted therapeutic strategies can improve health in the human metaorganism without negatively impacting the symbiotic relationships between microbes and host. Although traditional microbiome manipulating approaches such as antibiotics, prebiotics, probiotics, and fecal microbial transplantation have shown their own unique strengths and weaknesses, each of these present unique challenges particularly for use in chronic diseases such as end stage liver

disease. As we move toward selective nonlethal small molecule therapeutics, the goal is to have exquisite target selectivity and limited systemic drug exposure given that the targets are microbial in nature. This natural progression parallels the paradigm shifts in oncology which have transitioned from broadly cytotoxic chemotherapies to target-selective small molecule and biologics-based therapeutics. Here we provide the first evidence that the gut microbial choline metabolite TMA is elevated in the plasma of patients with AH, which corroborates previous reports showing that TMA is also prominent in the breath of patients with AH[40]. Hence, further studies are warranted to determine whether combined measures of breath and blood TMA can serve as a prognostic biomarker to accurately predict AH-related mortality. Here we also show for the first time that a selective nonlethal small molecule drug that reduces bacterial production of TMA can prevent ethanol-induced liver injury in mice. We also demonstrate that direct administration of TMA can elicit rapid signaling effects in the liver, supporting the notion that gut microbial metabolites produced postprandially can act in an endocrine-like manner to alter host signal transduction and associated disease pathogenesis. Collectively, these studies suggest that selective drugs targeting the gut microbial TMA pathway may hold promise for treating AH.

As drug discovery advances in the area of small molecule nonlethal bacterial enzyme inhibitors it is key to understand how these drugs impact microbial ecology in the gut and other microenvironments. As we have previously reported[27,29,30], gut microbe-targeted choline TMA lyase inhibitors (IMC and FMC) induced a significant remodeling of the cecal microbiome in mice. In the current studies there were some consistent, but many different cecal microbiome alterations when comparing IMC and FMC (Figure 4), yet both drugs similarly improved ethanol-induced liver injury. As small molecule bacterial enzymes inhibitors are developed it will be extremely important to understand their effects on microbial ecology, and it is expected that some of the beneficial effects of these drugs will indeed originate from the restructuring of gut

microbiome communities. In fact, this is not an uncommon mechanism by which host targeted drugs impact human health. A recent study showed that nearly a quarter of commonly used host-targeted drugs have microbiome-altering properties[71], and in the context of diabetes therapeutics it is important to note metformin's anti-diabetic effects are partially mediated by the drug's microbiome altering properties[72]. Given the strong association between gut microbiome and liver disease[3-22], it may prove advantageous to find therapeutics that beneficially remodel the gut microbiome as well as engage either their microbe or host target of interest.

The metaorganismal TMA/TMAO pathway represents only one of many microbial metabolic circuits that have been associated with human disease. In fact, many microbe-associated metabolites such as short chain fatty acids, secondary bile acids, phenolic acids, polyamines, and others have more recently been associated with many human diseases[21,22]. In an ethanol- and meal-related manner gut microbes produce a diverse array of metabolites that reach micromolar to millimolar concentrations in the blood, making the collective gut microbiome an active endocrine organ[21]. Small molecule metabolites are well known to be mediators of signaling interactions in the host, and this work provides evidence that diet/ethanol-microbe-host metabolic interplay can be causally linked to ethanol-induced liver injury. Our work, and that of many others, demonstrates that there is clear evidence of bi-directional crosstalk between the gut microbial endocrine organ and host liver metabolism. As drug discovery advances it will be important to move beyond targets based solely in the human host. This work highlights that non-lethal gut microbe-targeted enzyme inhibitors may serve as effective therapeutics in AH and provides proof of concept that this may be a generalizable approach to target metaorganismal crosstalk in other disease contexts. In fact, selective inhibition of bacterial enzymes has the advantage over host targeting given that small molecules can be designed to avoid systemic absorption and exposure, thereby minimizing potential host off target effects. As shown here

with the gut microbial TMA/TMAO pathway, it is easy to envision that other microbe-host interactions are mechanistically linked to host disease pathogenesis, serving as the basis for the rational design of microbe-targeted therapeutics that improve human health.

MATERIALS AND METHODS

Key Resources Table

Reagent type (species) or resource	Designation	Source or reference	Identifiers	Additional information
strain, strain background Mice, (Females)	9-11 Weeks	Jackson Laboratories	C57BL6/J	5-8 per study
biological sample (Humans)	Plasma samples from 285 patients	Cleveland Clinic Foundation; University of Louisville; University of Massachusetts Medical School; University of Texas Southwestern Medical Center	Not provided	
biological sample (Humans)	Liver samples from 5 healthy donors	Clinical Resource for Alcoholic Hepatitis Investigations at Johns Hopkins University	Not provided	

biological sample (Humans)	Liver samples from 5 patients with severe AH	Clinical Resource for Alcoholic Hepatitis Investigations at Johns Hopkins University	Not provided	
antibody	anti- FMO3 (Rabbit monoclonal)	Abcam	Cat# ab126790	1:1000 (WB)
antibody	anti-HSC70 (Mouse monoclonal)	Santa Cruz Biotechnology	Cat# sc-7298	1:1000 (WB)
antibody	Anti-rabbit IgG HRP	GE-Healthcare	Cat#: NA934-100UL	1:5000 (WB)
antibody	Anti-Mouse IgG HRP	GE-Healthcare	NA931VS	1:5000 (WB)
sequence-based reagent	Mouse Tnfα	Sigma	PCR primers	F:CCACCACG CTCTTCTGTC TAC R:AGGGTCTG GGCCATAGA ACT
sequenced-based reagent	Mouse Il1β	Sigma	PCR primers	F:AGTTGACG GACCCCAAA AG R:AGCTGGAT GCTCTCATCA GG
sequenced-based reagent	Mouse Fmo3	Sigma	PCR primers	F:CCCACATG CTTTGAGAG GAG

				R:GGAAGAGTTGGTGAAGACCG
sequenced-based reagent	Mouse Taar5	Sigma	PCR primers	F:AAAGAAAAGCTGCCAAGA R:AAGGGAAGCCAACACACA
sequenced-based reagent	Mouse CyclophilinA	Sigma	PCR primers	F:GCGGCAGGTCCATCTACG R:GCCATCCAGCCATTCAGTC
sequenced-based reagent	Mouse Cxcl1	IDT	PCR primers	F:TGCACCCAAACCGAAGTC R:GTCAGAAGCCAGCGTTCACC
sequenced-based reagent	Mouse Grp78	IDT	PCR primers	F:ACTTGGGGACCACCTATTCCT R:ATCGCCAATCAGACGCTCC
commercial assay or kit	AST Commercial Kit	Sekisui Diagnostics	319-30	
commercial assay or kit	ALT Commercial Kit	Sekisui Diagnostics	318-30	
commercial assay or kit	Triglyceride Commercial Kit	Wako	994-02891	
commercial assay or kit	Total Cholesterol Commercial Kit	Fisher Scientific	TR134321	
commercial assay or kit	Free Cholesterol	Wako	993–02501	

	Commercial Kit			
commercial assay or kit	RNAeasy Lipid Tissue Mini Kit	Qiagen	74804	
commercial assay or kit	Thermo Scientific™ Pierce™ TiO2 Phosphopeptide Enrichment and Clean-up Kit	Fisher Scientific	PI88301	
commercial assay or kit	RNAeasy Purification Kit	Qiagen	74004	
chemical compound, drug	Iodomethylcholine (IMC)	Synthesized at the Cleveland Clinic	Not provided	
chemical compound, drug	Fluoromethylcholine (FMC)	Synthesized at the Cleveland Clinic	Not provided	
chemical compound, drug	Trimethylamine Hydrochloride	Sigma	T72761	
chemical compound, drug	Lipopolysaccharide	Sigma	L4391	
software, algorithm	Graphpad Prism	GraphPad Software, Inc.	8.4	
software, algorithm	DADA2	https://benjjneb.github.io/dada2/dada-installation.html	1.16	

software, algorithm	Phyloseq	https://www.bioconductor.org/packages/release/bioc/html/phyloseq.html	4.1	
software, algorithm	microbiomeSeq	https://github.com/umerijaz/microbiomeSeq	1	
software, algorithm	Ggplot2	https://cran.r-project.org/web/packages/ggplot2/index.html	3.3.5	
software, algorithm	vegan	https://cran.r-project.org/web/packages/vegan/index.html	2.5-7	
other	Supersignal West Pico Plus Substrate	Thermo Fisher	34577	
other	Diet	Dyets	710260	

Overview of Human Study Populations

We made use of 3 different human study populations, detailed below, that included patients with severities of AH/ALD It must be noted that one limitation of our study is that each of these cohorts used slightly different diagnostic criteria for defining the severity/stage of AH/ALD.

Human Study Populations and Sample Collection for TMA Measurement

A total of 285 subjects were included in this study. De-identified plasma samples, along with clinical and demographic data, were obtained from 1) the Northern Ohio Alcohol Center (NOAC) at the Cleveland Clinic biorepository including 21 healthy individuals and 15 patients diagnosed

and 2) the Defeat Alcoholic Steatohepatitis (DASH) consortium (Cleveland Clinic, University of Louisville School of Medicine, University of Massachusetts Medical School, and University of Texas Southwestern Medical Center) including 249 patients with AH. Diagnosis with AH was performed using clinical and laboratory criteria, with MELD score utilized for distinguishing moderate (MELD<20) and severe (MELD≥20) AH, as recommended by the NIAAA Alcoholic Hepatitis consortia[42]. A detailed description of patient recruitment, inclusion and exclusion criteria for the DASH consortium has been reported in previous studies[50]. Patients with AH were classified as moderate (MELD < 20, n=112) and severe (MELD ≥20, n=152) according to the MELD score at admission as part of either of two independent clinical trials (ClincalTrials.gov identifier # NCT01809132 and NCT03224949) or the NOAC biorepository. These studies were approved by the Institutional Review Boards of all 4 participating institutions and all study participants consented prior to collection of data and blood samples. Clinical and demographic data for the entire cohort is presented in Figure 1-Table Supplement 1 and for the sub-set of subjects used for TMA analysis is presented in Figure 1-Table Supplement 2.

In order to be able to measure volatile compounds such as trimethylamine (TMA), blood was collected in EDTA-coated tubes and immediately placed on ice. Plasma was separated by centrifugation at 1200 x g for 15 minutes at 4°C. Plasma was rapidly acidified by adding 25 mL of 1 M hydrochloric acid (HCL) to 500 mL of aliquoted plasma, followed by vigorous vortexing. Acidified plasma samples were stored at -80°C in air-tight O-ring cryovials (Fisher Scientific, product # 02-681-373) until being processed for quantification of TMA and other volatile compounds. A non-acidified sample was also collected for standard plasma biochemistries.

Analysis of Hepatic FMO3 Expression across Different Liver Disease Etiologies

For data shown in main Figure 1 panel C, we leveraged access to publicly available bulk liver RNA sequencing data from patients with different liver disease etiologies[43]. For this cohort, early AH (EAH) was defined as MELD 7-8, severe AH with liver failure (AHL) with MELD 22-28, and AHL with emergency liver transplant (ExAH) with MELD 18-21. All raw fastq files were downloaded from SRA (PRJNA531223) and dbGAP (phs001807.v1.p1)[43]. Fastq files were aligned to the human genome (GRCh38, indices downloaded from https://github.com/pachterlab/kallisto-transcriptome-indices/releases/download/ensembl-96/homo_sapiens.tar.gz) using Kallisto version 0.44.0 with 100 bootstraps calculated[73]. Data were then merged with clinical data and analyzed with Sleuth in gene_mode with aggregation_column set to Ensemble Gene ID; in addition, extra_bootstrap_summary and read_bootstrap_tpm were set to true[74]. Differential expression was measured with Sleuth using a cutoff of $q<0.05$.

Human Study Populations and Sample Collection for Liver Western Blotting

De-identified samples from five livers explanted from severe AH patients during liver transplantation or five wedge biopsies from healthy donor livers were snap frozen in liquid nitrogen and stored at -80°C. Samples were provided by the Clinical Resource for Alcoholic Hepatitis Investigations at Johns Hopkins University (R24 AA0025107, Z. Sun PI). Written informed consent was obtained from each patient included in the study and the study protocol conforms to the ethical guidelines of the 1975 Declaration of Helsinki as reflected in a priori approval by the Institutional Review Boards at Johns Hopkins Medical Institutions. This cohort utilized Maddrey's Discriminant Function as the primary indicator of disease severity, with an average score of 102.5 $\pm$ 27.7. MELD scores are not available for this cohort. Descriptive biochemical and clinical data for this cohort have been reported previously[7].

Immunoblotting

Whole tissue homogenates were made from tissues in a modified RIPA buffer as previously described[44-47], and protein was quantified using the bicinchoninic (BCA) assay (Pierce). Proteins were separated by 4–12% SDS-PAGE, transferred to polyvinylidene difluoride (PVDF) membranes, and then proteins were detected after incubation with specific antibodies as previously described[44-47] and listed in the Key Resources Table.

Real-Time PCR Analysis of Gene Expression

Tissue RNA extraction and qPCR analysis was performed as previously described[45]. The mRNA expression levels were calculated based on the ΔΔ-CT method using cyclophilin A as the housekeeping gene. qPCR was conducted using the Applied Biosystems 7500 Real-Time PCR system. All primer sequences are listed in the Key Resources Table.

Chemical Synthesis of Gut Microbe-Targeted Choline TMA Lyase Inhibitors

The small molecule choline TMA lyase inhibitors iodomethylcholine (IMC) and fluoromethylcholine (FMC) have been previously described as potent and selective mechanism-based inhibitors targeted microbial CutC[27]. Here, IMC and FMC were synthesized and structurally characterized as outlined below using both multinuclear NMR analysis and high-resolution mass spectrometry. ^{1}H and ^{13}C-NMR spectra for IMC and FMC were recorded on a Bruker Ascend spectrometer operating at 400 MHz. Chemical shifts are reported as parts per million (ppm). Iodomethylcholine iodide was prepared using a previously reported method using 2-dimethylethanolamine and diiodomethane as reactants in acetonitrile followed by recrystallization from dry ethanol. ^{1}H- and ^{13}C-NMRs of IMC were both consistent with that in the

reported literature[75], as well as consistent based on proton and carbon chemical shift assignments indicated below. High resolution MS corroborated the expected cation mass and provided further evidence of structural identity. ^{1}H-NMR (400 MHz, D_2O): 5.24 (s, 2H, -N-C$\underline{H}_2$-I), 4.06-3.99 (m, 2H, -CH_2-C$\underline{H}_2$-OH), 3.68-3.62 (m, 2H, -N-C$\underline{H}_2$-CH_2-), 3.29 (s, 6H, -N(C$\underline{H}_3$)$_2$); ^{13}C-NMR (100 MHz, D_2O): 66.1 (-CH_2-$\underline{C}H_2$-OH), 55.8 (-N-$\underline{C}H_2$-CH_2-), 52.9 (-N($\underline{C}H_3$)$_2$), 33.0 (-N-$\underline{C}H_2$-I); HRMS (ESI/TOF): m/z (M^+) calculated for $C_5H_{13}INO$, 230.0036; found, 230.0033. The synthesis of fluoromethylcholine chloride was performed using the procedure below. ^{1}H- and ^{13}C-NMRs of FMC were consistent with that in the reported literature[12]. High resolution MS was also consistent with the expected cation mass. Chloro(fluoro)methane (2.05 kg, 29.9 mol, 6 eq) was bubbled into a solution of 2-dimethylaminoethanol (444.0 g, 4.98 mol, 500 mL, 1 eq) in THF (1000 mL) at -70 ^{o}C for 4 h. The mixture was then transferred to an autoclave and heated to 80 ^{o}C and stirred for 18 h (pressure: ~15-50 psi). During this period, a white precipitate formed. The solid was isolated by filtration, washed with cold THF (600 mL), and dried under vacuum to give fluoromethylcholine chloride as a white solid (1.14 kg, 70.7% yield, 98.0 % purity). ^{1}H-NMR (400 MHz, D_2O): 5.44 (s, 1H, -N-C$\underline{H}_2$-F), 5.32 (s, 1H, -N-C$\underline{H}_2$-F), 4.04-3.98 (m, 2H, -CH_2-C$\underline{H}_2$-OH), 3.60-3.54 (m, 2H, -N-C$\underline{H}_2$-CH_2-), 3.19 (s, 6H, -N(C$\underline{H}_3$)$_2$); ^{13}C-NMR (100 MHz, D_2O): 97.8 and 95.6 (-N-$\underline{C}H_2$-F), 62.9 (-CH_2-CH_2-OH), 55.1 (-N-CH_2-CH_2-), 48.0 (-N(CH_3)$_2$); HRMS (ESI/TOF): m/z (M^+) calculated for $C_5H_{13}FNO$ (M^+) 122.0976, found 122.0975.

Ethanol Feeding Trials in Mice

All mice were maintained in an Association for the Assessment and Accreditation of Laboratory Animal Care, International-approved animal facility. All experimental protocols were approved by the institutional animal care and use committee (IACUC) at the Cleveland Clinic. Age- and weight-matched female C57BL6/J mice were randomized into pair- and ethanol-fed groups and

adapted to control liquid diet for 2 days. Two models of chronic ethanol feeding were used. 1) A 25 day chronic model in which mice were allowed free access to increasing concentrations of ethanol for 25 days (i.e chronic feeding model) as previously described[48]. In this model, the ethanol-fed mice were acclimated to ethanol as follows: 1% vol/vol for 2 days, 2% vol/vol for 2 days, 4% vol/vol (22% kcal) for 1 wk, 5% vol/vol (27% kcal) for 1 wk, and last 6% vol/vol (32% kcal) for 1 wk and is denoted as 32%, *day 25*. 2) A 10 day chronic model in which mice were allowed free access to a 5% vol/vol (27% kcal) for 10 days[76]. Ethanol-fed mice were allowed ad libitum access to liquid diet. Control mice were pair fed a diet that received isocalorically substituted maltose dextrin for ethanol. Some cohorts received choline TMA lyase inhibitors IMC (0.06% wt/wt) or FMC (0.006% wt/wt) in these liquid diets throughout the entire 10-25 day feeding period. Lieber-DeCarli high-fat ethanol and control diets were purchased from Dyets (catalog no.710260; Bethlehem, PA).

Lipopolysaccharide (LPS) Injections

Female C57BL6/J mice at 10.5 weeks old were injected intraperitoneally with either 15mg/kg Lipopolysaccharide (500ug/mL, Sigma L4391) or a matched volume (30mL/kg) of sterile saline. After 6 hours, mice were euthanized with ketamine/xylazine and the liver was immediately collected and homogenized in TRIzol. RNA was extracted using chloroform phase separation and purified using Qiagen RNeasy kit.

Liver Histology and Immunohistochemistry

For histological analysis, formalin-fixed tissues were paraffin embedded, sectioned, and stained with hematoxylin and eosin. Formalin-fixed samples are coded at the time of collection for blinded analysis.

Measurement of Plasma Aminotransferase Levels

To determine the level of hepatic injury in mice, plasma was used to quantify alanine (ALT) and aspartate (AST) aminotransferase levels using a commercially available enzymatic assay (Sekisui Diagnostics, Lexington, MA, USA) according to manufacturer's instruction.

Measurement of Hepatic Lipid Levels

Extraction of liver lipids and quantification of total plasma and hepatic triglycerides, cholesterol, and cholesterol esters was conducted using enzymatic assays as described previously[44-47].

Quantification of Trimethyamine (TMA)-Related Metabolites in Acidified Plasma

Stable isotope dilution high performance liquid chromatography with on-line tandem mass spectrometry (LC–MS/MS) was used for quantification of levels of TMAO, TMA, choline, carnitine, betaine, and γ-butyrobetaine in plasma, as previously described[49]. Their d_9(methyl)-isotopologues were used as internal standards. LC–MS/MS analyses were performed on a Shimadzu 8050 triple quadrupole mass spectrometer. IMC and d_2-IMC, along with other metabolites, were monitored using multiple reaction monitoring of precursor and characteristic product ions as follows: m/z 230.0 → 58.0 for IMC; m/z 232.0 → 60.1 for d_2-IMC; m/z 76.0 → 58.1 for TMAO; m/z 85.0 → 66.2 for d_9-TMAO; m/z 60.2 → 44.2 for TMA; m/z 69.0 → 49.1 for d_9-TMA; m/z 104.0 → 60.1 for choline; m/z 113.1 → 69.2 for d_9-choline; m/z 118.0 → 58.1 for betaine; m/z 127.0 → 66.2 for d_9-betaine.

Cecal Microbiome Analyses

16S rRNA amplicon sequencing were done for V4 region using via miSEQ from mouse cecal contents. Raw 16S amplicon sequence and metadata, were *demultiplexed using split_libraries_fastq*.py script implemented *in QIIME1.9.1*[78]*.* Demultiplexed fastq file was split into sample specific fastq files using split_sequence_file_on_sample_ids.py script from Qiime1.9.1[78]. Individual fastq files without non-biological nucleotides were processed using Divisive Amplicon Denoising Algorithm (DADA) pipeline[79]. The output of the dada2 pipeline (feature table of amplicon sequence variants (an ASV table)) was processed for alpha and beta diversity analysis using *phyloseq*[77], and microbiomeSeq (http://www.github.com/umerijaz/microbiomeSeq) packages in R. Alpha diversity estimates were measured within group categories using estimate_richness function of the *phyloseq* package[77]. Multidimensional scaling (MDS, also known as principal coordinate analysis; PCoA) was performed using Bray-Curtis dissimilarity matrix[20]. between groups and visualized by using *ggplot2* package[80]. We assessed the statistical significance ($P < 0.05$) throughout and whenever necessary, we adjusted *P*-values for multiple comparisons according to the Benjamini and Hochberg method to control False Discovery Rate[81] while performing multiple testing on taxa abundance according to sample categories. We performed an analysis of variance (ANOVA) among sample categories while measuring the of α-diversity measures using plot_anova_diversity function in *microbiomeSeq* package (http://www.github.com/umerijaz/microbiomeSeq). Permutational multivariate analysis of variance (PERMANOVA) with 999 permutations was performed on all principal coordinates obtained during PCoA with the *ordination* function of the *microbiomeSeq* package. Wilcoxon (Non-parametric) test were performed on ASVs abundances against meta-data variables levels using their base functions in R[82].

RNA Sequencing in Mouse Tissues

RNA-Seq libraries were generated from mouse liver using the Illumina mRNA TruSeq Directional library kit and sequenced using an Illumina HiSeq4000 (both according to the Manufacturer's instructions). RNA sequencing was performed by the University of Chicago Genomics Facility, and data analysis and data availability are described in detail in the online supplement. Briefly, RNA samples were checked for quality and quantity using the Bio-analyzer (Agilent). RNA-SEQ libraries were generated using the Illumina mRNA TruSEQ Directional library kit and sequenced using an Illumina HiSEQ4000 (both according to the Manufacturer's instructions). RNA sequencing was performed by the University of Chicago Genomics Facility. Raw sequence files will be deposited in the Sequence Read Archive before publication (SRA). Single-end 100 bp reads were trimmed with Trim Galore (v.0.3.3, http://www.bioinformatics.babraham.ac.uk/projects/trim_galore) and controlled for quality with FastQC (v0.11.3, http://www.bioinformatics.bbsrc.ac.uk/projects/fastqc) before alignment to the Mus musculus genome (Mm10 using UCSC transcript annotations downloaded July 2016). Reads were aligned using the STAR alignerSTAR in single pass mode (v.2.5.2a_modified, https://github.com/alexdobin/STAR) with standard parameters. Raw counts were loaded into R (http://www.R-project.org/) (R Development Core Team, 2015) and edgeR was used to perform upper quantile, between-lane normalization, and DE analysis. Values generated with the cpm function of edgeR, including library size normalization and log2 conversion, were used in figures. Heat maps were generated of top 50 differentially expressed transcripts using pheatmap. Reactome-based pathway analysis was performed using an open-sourced R package: ReactomePA. RNA sequencing data have been deposited into the National Institutes of Health (NIH)-sponsored GEO repository (Accession number GSE157681).

Phosphoproteomics Analyses to Examine TMA-Induced Signaling Events in Mouse Liver

The goal of this experiment was to unbiasedly identify TMA-responsive signaling events in mouse liver after an acute exposure (10 minutes) of TMA. To closely mimic physiological route of delivery, we delivered saline or TMA directly into the portal vein in fasted mice. Briefly, C57BL/6 mice were fasted overnight (12 hour fast), and between the hours of 9:00–10:00 am (2–3 hours into light cycle), mice were anesthetized using isoflurane (4% for induction and 2% for maintenance). Once fully anesthetized, a midline laparotomy was performed, and the portal vein was visualized under a Leica M650 surgical microscope. Briefly, a fresh 10 mM stock of trimethylamine-hydrochloride (TMA-HCL) made in sterile saline, and the pH of stock solution was adjusted to 7.4. Mice then received 20 µl of either saline vehicle or TMA-HCL via direct syringe infusion (Becton-Dickson product # 309306). 9.75 minutes later a small aliquot (~50 µl) of portal blood was collected by pulling back on injection syringe left in place following injection. In saline vehicle injected mice, portal blood levels of TMA ranged from 0.49–2.22 µM and TMAO levels ranged from 2.53–7.14 µM. In mice injected with TMA-HCL, portal blood levels of TMA ranged from 125.36–319.55 µM and TMAO levels ranged from 9.68–17.48 µM. Exactly 10 minutes after initial injection, the liver was rapidly snap frozen by immersion in liquid nitrogen. Liver samples were homogenized, the protein was precipitated with acetone, and the protein concentration was measured. A total of 1 mg of protein from each sample was digested with trypsin and the resulting tryptic peptides were subjected to phosphoserine and phosphothreonine enrichment using the Thermo Scientific™ Pierce™ TiO_2 Phosphopeptide Enrichment and Clean-up Kit (Fisher # PI88301). The enrichment was performed based on the manufacturer's instructions. The enriched peptide samples were subjected to C18 clean-up prior to LC-MS analysis. The LC-MS system was a Finnigan LTQ-Obitrap Elite hybrid mass spectrometer system. The HPLC column was a Dionex 15 cm x 75 µm id Acclaim Pepmap C18, 2µm, 100 Å reversed- phase capillary chromatography column. Five µL volumes of the extract

were injected and the peptides eluted from the column by an acetonitrile/0.1% formic acid gradient at a flow rate of 0.25 µL/min were introduced into the source of the mass spectrometer on-line. The microelectrospray ion source is operated at 1.9 kV. The digest was analyzed using the data dependent multitask capability of the instrument acquiring full scan mass spectra to determine peptide molecular weights and product ion spectra to determine amino acid sequence in successive instrument scans. The LC-MS/MS data files were searched against the mouse UnitProtKB database (downloaded in Dec 2019 contains 17017 sequences) using Sequest bundled into Proteome Discoverer 2.4. Cysteine carbamidomethylation was set as a fixed modification and oxidized methionine, protein N-terminal acetylation, and phosphorylation of Serine, Threonine, and Tyrosine were considered as dynamic modification. A maximum of two missed cleavages were permitted. The peptide and protein false discovery rates were set to 0.01 using a target-decoy strategy. Phosphorylation sites were identified using ptmRS node in PD2.4. The relative abundance of the positively identified phosphopeptides was determined using the extracted ion intensities (Minora Feature Detection node) with Retention time alignment. All peptides were included in the quantitation, the peptide intensities were normalized to total peptide amount. Missing values were imputed in Perseus using a normal distribution. A total of 789 phosphopeptides were identified with 36 phosphopeptides determined to be two-fold different in the TMA and Saline samples with a p-value <0.05 (t-test).

Statistical Analysis

All statistical analysis were performed using Graphpad Prism and $P < 0.05$ was considered statistically significant. All data are presented as mean ± SEM, unless otherwise noted in the figure legends. All data were tested for equal variance and normality. For 2-group comparison of parametric data, a two-tailed Student's *t*-test was performed, while nonparametric data were

analyzed with Mann-Whitney U test (also called the Wilcoxon rank sum test). For studies comparing vehicle and TMA lyase inhibitors in pair- and ethanol-fed mice, a two-way analysis of variance (ANOVA) was performed, followed by Tukey's tests for post hoc analysis. For human studies in AH patients, statistical significance was determined by analysis of variance and a Tukey's honest significant difference post-hoc test ($P < .05$).

ACKNOWLEDGEMENTS

This work was supported in part by National Institutes of Health grants P50 AA024333 (A.J.M., S.D., D.S.A., L.E.N., J.M.B.), R01 DK120679 (J.M.B.), P01 HL147823 (J.M.B., S.L.H.), U01 AA026938 (L.E.N., J.M.B.), P50 CA150964 (J.M.B.), U01 AA021890 (L.E.N., S.D.), U01 AA021893 (S.D., B.B., C.J.M., M.M., G.S., and A.J.M.), R01 HL103866 (S.L.H.), R01 HL144651 (Z.W.), R01 HL130819 (Z.W.), U01 AA026980 (C.J.M.), P50 AA 024337 (C.J.M.), R21 AR 071046 (S.D.), R01 GM119174 (S.D.), R01 DK113196 (S.D.), R56 HL141744 (S.D.), U01 DK061732 (S.D.), U01 AA026977 (G.S.), UH3 AA026970 (G.S.), K99 AA028048 (A.K.), a Leducq Transatlantic Networks of Excellence Award (S.L.H.), a JSPS Overseas Research Fellowship 201960331 (T.M.), and the American Heart Association (Postdoctoral Fellowships 17POST3285000 to R.N.H and 15POST2535000 to R.C.S). The Orbitrap Elite instrument used for proteomics was purchased via an NIH shared instrument grant 1S10RR031537 (B.W.).

COMPETING FINANCIAL INTERESTS

T.M., A.K., V.V., N.S., E.H., R.B., A.L.B., K.K.F., W.M., C.N., D.O., L.J.O., R.C.S., M.R.M., A.B., K.L.P., A.K., V.P., M.M., J.T.A., B.W. C.J.M., M.M., A.J.M., S.R., B.B., S.D. D.M.R., D.S.A. L.E.N., and J.M.B. all declare no competing financial interests. R.N.H. reports being a paid consultant for the University of Cincinnati. Z.W. and S.L.H. report being named as co-inventor

on pending and issued patents held by the Cleveland Clinic relating to cardiovascular diagnostics and therapeutics. S.L.H. reports being a paid consultant for Zehna Therapeutics, having received research funds from Zehna Therapeutics, Procter & Gamble, and Roche Diagnostics. S.L.H. and Z.W. report being eligible to receive royalty payments for inventions or discoveries related to cardiovascular diagnostics or therapeutics from Zehna Therapeutics, Cleveland Heart Lab, a wholly owned subsidiary of Quest Diagnostics, and Procter & Gamble. G.S. reports being a paid consult for Allergan, Alnylam, Arrow, Durcect Corporation, Generon, Glympse Bio, Terra Firma, Quest Diagnostics, Pandion Therapeutics, Surrozen, and Zomagen. G.S. has received grants from Gilead, Genfit, Intercept, Novartis, SignaBlok, and Shire; she also holds intellectual property rights with Up to Date. J.C.G-G is an employee of The Procter & Gamble Co. J.A.B. reports being eligible to receive royalty payments for inventions or discoveries related to cardiovascular therapeutics from Zehna Therapeutics, and the Proctor & Gamble Co.

ABBREVIATIONS USED: AH, alcohol-associated hepatitis; ALD, alcohol-associated liver disease; CutC, choline trimethylamine lyase; CVD, cardiovascular disease; FMO3, flavin containing monooxygenase 3; FMC, fluoromethylcholine; IHC, immunohistochemical; IMC, iodomethylcholine; LPS, lipopolysaccharide; MELD, model for end-stage liver disease; MAMPs, microbe-associated molecular patterns; NMDS, Non-metric multidimensional scaling; PC, phosphatidylcholine; PCA, principal component analysis; TMA, trimethylamine; TMAO, trimethylamine N-oxide; TNFα, tumor necrosis factor alpha.

DATA AVAILABILITY STATEMENT

The data supporting the findings of this study are available within the article.

LITERATURE CITED:

1. Masarone M, Rosato V, Dallio M, Abenavoli L, Federico A, Loguercio C, Persico C. Epidemiology and natural history of alcoholic liver disease. Rev Recent Clin Trials 2016;11:167-174.
2. Kochanek KDMS, Xu JQ, Arias E. Deaths: final data for 2017. National vital statistics reports. Hyattsville (MD): National Center for Health Statistics.
3. Chen Y, Yang F, Lu H, Wang B, Chen Y, Lei D, et al. Characterization of fecal microbial communities in patients with liver cirrhosis. Hepatology 2011;54:562–572.
4. Yan AW, Fouts DE, Brandl J, Starkel P, Torralba M, Schott E, et al. Enteric dysbiosis associated with a mouse model of alcoholic liver disease. Hepatology 2011;53:96-105.
5. Mutlu E, Keshavarzian A, Engen P, Forsyth CB, Sikaroodi M, Gillevet P. Intestinal dysbiosis: a possible mechanism of alcohol-induced endotoxemia and alcoholic steatohepatitis in rat. Alcohol Clin Exp Res 2009;33:1836-1846.
6. Mutlu EA, Gillevet PM, Rangwala H, Sikaroodi M, Naqvi A, Engen PA, et al. Colonic microbiome is altered in alcoholism. Am J Physiol Gastrointest Liver Physiol 2012;302:G966–G978.
7. Tripathi A, Debelius J, Brenner DA, Karin M, Loomba R, Schnabl B, Knight R. The gut-liver axis and the intersection with the microbiome. Nat Rev Gastroenterol Hepatol 2018;15:397-411.
8. Ciocan D, Rebours V, Voican CS, Wrzosek L, Puchois V, Cassard AM, Perlemuter G. Characterization of intestinal microbiota in alcoholic patients with and without alcoholic hepatitis or chronic alcoholic pancreatitis. Sci Rep 2018;8:4822.

9. Llopis M, Cassard AM, Wrzosek L, Boschat L, Bruneau A, Ferrere G, Puchois V, et al. Intestinal microbiota contributes to individual susceptibility to alcoholic liver disease. Gut 2016;65:830–839.
10. Duan Y, Llorente C, Lang S, Brandl K, Chu H, Jiang L, White RC, et al. Bacteriophage targeting of gut bacterium attenuates alcoholic liver disease. Nature 2019;575:505–511.
11. Smirnova E, Puri P, Muthiah MD, Daitya K, Brown R, Chalasani N, et al. Fecal microbiome distinguishes alcohol consumption from alcoholic hepatitis but does not discriminate disease severity. Hepatology 2020;72:271-286.
12. Gao B, Lang S, Duan Y, Wang Y, Shawcross DL, Louvet A, et al. Serum and fecal oxylipins in patients with alcohol-related liver disease. Dig Dis Sci 2019;1878–1892.
13. Puri P, Liangpunsakul S, Christensen JE, Shah VH, Kamath PS, Gores GJ, et al. The circulating microbiome signature and inferred functional metagenomics in alcoholic hepatitis. Hepatology. 2018;67:1284–1302.
14. Lang S, Schnabl B. Microbiota and fatty liver disease – the known, unknown, and the future. Cell Host Microbe 2020; 28:233-244.
15. Wilkinson SP, Arroyo V, Gazzard BG, Moodie H, Williams R. Relation of renal impairment and hemorrhagic diathesis to endotoxemia in fulminant liver failure. Lancet 1974;1:521-524.
16. Tarao K, Muroi T, Nagakura Y, Ikeuchi T, Suyama T, Endo O, Fukushima K. Relationship between endotoxemia and protein concentration of ascites in cirrhotic patients. Gut 1979;20:205-210.
17. Uesugi T, Froh M, Arteel GE, Bradford BU, Thurman RG. Toll-like receptor 4 is involved in the mechanism of early alcohol-induced liver injury in mice. Hepatology 2001;34:101-108.

18. Paik YH, Schwabe RF, Bataller R, Russo MP, Jobin C, Brenner DA. Toll-like receptor 4 mediates inflammatory signaling by bacterial lipopolysaccharide in human hepatic stellate cells. Hepatology 2003;37:1043-1055.
19. DeSantis DA, Ko CW, Liu Y, Liu X, Hise AG, Nunez G, Croniger CM. Alcohol-induced liver injury is modulated by Nlrp3 and Nlrc4 inflammasomes in mice. Mediators Inflamm 2013;2013:751374.
20. Knorr J, Wree A, Tacke F, Feldstein AE. The NLRP3 inflammasome in alcoholic and nonalcoholic steatohepatitis. Semin Liver Dis 2020;40:298-306.
21. Brown JM, Hazen SL. The gut microbial endocrine organ: bacterially derived signals driving cardiometabolic diseases. Annu Rev Med 2015;66:343-359.
22. Gilbert JA, Blaser MJ, Caporaso JG, Jansson JK, Lynch SV, Knight R. Current understanding of the human microbiome. Nat Med 2018;24:392-400.
23. Kwak DS, Jun DW, Seo JG, Chung WS, Park S-E, Lee KN, et al. Short-term probiotic therapy alleviates small intestinal bacterial overgrowth, but does not improve intestinal permeability in chronic liver disease. Eur J Gastroenterol Hepatol 2014;26:1353-1359.
24. Asgharian H, Homayouni-Rad A, Mirghafourvand M, Mohammad-Alizadeh-Charandabi S. Effect of probiotic yoghurt on plasma glucose in overweight and obese pregnant women: a randomized controlled clinical trial. Eur J Nutr 2020;59, 205-215.
25. Reijinders D, Goossens GH, Hermes GD, Neis EPJG, Van Der Beek CM, Most J, et al. Effects of gut microbiota manipulation by antibiotics on host metabolism in obese humans: A randomized double-blind placebo-controlled trial. Cell Metab 2016;24:63-74.
26. Madjd A, Taylor MA, Mousavi N, Delavari A, Malekzadeh R, Macdonald IA, Farshchi HR. Comparison of the effect of daily consumption of probiotic compared with low-fat

conventional yogurt on weight loss in healthy obese women following an energy-restricted diet: a randomized controlled trial. Am J Clin Nutr 2016;103:323-329.

27. Roberts AB, Gu X, Buffa JA, Hurd AG, Wang Z, Zhu W, et al. Development of a gut microbe-targeted nonlethal therapeutic to inhibit thrombosis potential. Nat Med 2018;24:1407-1417.
28. Wang Z, Roberts AB, Buffa JA, Levison BS, Zhu W, Org E, et al. Non-lethal inhibition of gut microbial trimethylamine production for the treatment of atherosclerosis. Cell 2015:163:1585-1595.
29. Gupta N, Buffa JA, Roberts AB, Sangwan N, Skye SM, Li L, et al. Targeted inhibition of gut microbial trimethylamine N-oxide production reduces renal tubulointerstitial fibrosis and functional impairment in a murine model of chronic kidney disease. Arterioscler Thromb Vasc Biol 2020;40:1239-1255.
30. Organ CL, Li Z, Sharp TE 3rd, Polhemus DJ, Gupta N, Goodchild TT, et al. Nonlethal inhibition of gut microbial trimethylamine N-oxide production improves cardiac function and remodeling in a murine model of heart failure. J Am Heart Assoc 2020:9:e016223.
31. Orman M, Bodea S, Funk MA, Martinez-del Campo A, Bollenbach M, Drennan CL, Balskus EP. Structure-guided identification of a small molecule that inhibits anaerobic choline metabolism by human gut bacteria. J Am Chem Soc 2019;141:33-37.
32. Wang Z, Klipfell E, Bennett BJ, Koeth R, Levison BS, DuGar B, et al. Gut flora metabolism of phosphatidylcholine promotes cardiovascular disease. Nature 2011;472:57-63.
33. Koeth R, Wang Z, Levison BS, Buffa JA, Org E, Sheehy BT, et al. Intestinal microbiota metabolism of L-carnitine, a nutrient in red meat, promotes atherosclerosis. Nat Med 2013;19: 576-585.

34. Zhu W, Gregory JC, Org E, Buffa JA, Gupta N, Wang Z, et al. Gut microbial metabolite TMAO enhances platelet hyperreactivity and thrombosis risk. Cell 2016;165:111-124.
35. Zhu W, Wang Z, Tang WHW, Hazen SL. Gut microbe-generated trimethylamine N-oxide from dietary choline is prothrombotic in subjects. Circulation 2017;135:1671-1673.
36. Tang WHW, Wang Z, Levinson B, Koeth RA, Britt EB, Xiaoming F, et al. Intestinal microbial metabolism of phosphatidylcholine and cardiovascular disease risk. N Engl J Med 2013;368:1575-1584.
37. Wang Z, Tang WH, Buffa JA, Fu X, Britt EB, Koeth RA, et al. Prognostic value of choline and betaine depends on intestinal microbiota-generated metabolite trimethylamine-N-oxide. Eur Heart J 2014;35:904-910.
38. Trøseid M, Ueland T, Hov JR, Svardal A, Gregersen I, Dahl CP, et al. Microbiota-dependent metabolite trimethylamine-N-oxide is associated with disease severity and survival of patients with chronic heart failure. J Intern Med 2015;277:717-720.
39. Tang WH, Hazen SL. The contributory role of gut microbiota in cardiovascular disease. J Clin Invest 2014;124:4204-4211.
40. Hanouneh IA, Zein NN, Cikach F, Dababneh, L, Grove D, Alkhouri N, et al. The breathprints in patients with liver disease identify novel breath biomarkers in alcoholic hepatitis. Clin Gastroenterol Hepatol 2014;12:516-523.
41. Ascha M, Wang Z, Ascha MS, Dweik R, Zein NN, Grove D, et al. Metabolomics studies identify novel diagnostic and prognostic indicators in patients with alcoholic hepatitis. World J Hepatol 2016;8:499-508.
42. Crabb DW, Bataller R, Chalasani NP, Kamath PS, Lucey M, Mathurin P, et al. Standard Definitions and Common Data Elements for Clinical Trials in Patients With Alcoholic

Hepatitis: Recommendation From the NIAAA Alcoholic Hepatitis Consortia. Gastroenterology 2016;150:785-790.

43. Argemi J, Latasa MU, Atkinson SR, Blokhin IO, Massey V, Gue JP, et al. Defective HNF4alpha-dependent gene expression as a driver of hepatocellular failure in alcoholic hepatitis. Nat Commun 2019;1:3126.
44. Warrier M, Shih DM, Burrows AC, Ferguson D, Gromovsky AD, Brown AL, et al. The TMAO-generating enzyme flavin monooxygenase 3 is a central regulator of cholesterol balance. 2015;10:326-338.
45. Helsley RN, Varadharajan V, Brown AL, Gromovsky AD, Schugar RC, Ramachandiran I, et al. Obesity-linked suppression of membrane-bound O-acyltransferase 7 (MBOAT7) drives non-alcoholic fatty liver disease progression. Elife 2019;8:e49882.
46. Schugar RC, Shih DM, Warrier M, Helsley RN, Burrows A, Ferguson D, et al. The TMAO-producing enzyme flavin-containing monooxygenase 3 regulates obesity and the beiging of white adipose tissue. Cell Rep. 2017;19:2451-2461.
47. Lord CC, Ferguson D, Thomas G, Brown AL, Schugar RC, Burrows A, et al. Regulation of hepatic triacylglycerol metabolism by CGI-58 does not require ATGL co-activation. Cell Rep. 2016;16:939-949.
48. McCullough RL, McMullen MR, Sheehan MM, Poulsen KL, Roychowdhury S, Chiang DJ, et al. Complement factor D protects mice from ethanol-induced inflammation and liver injury. Am J Physiol. Gastrointest Liver Physiol 2018;315:G66-G79.
49. Wang Z, Levison BS, Hazen JE, Donahue L, Li XM, Hazen SL. Measurement of trimethylamine-N-oxide by stable isotope dilution liquid chromatography tandem mass spectrometry. Anal Biochem 2014;15:35-40.

50. Vatsalya V, Cave MC, Kong M, Gobejishvili L, Falkner KC, Craycroft J, et al. Keratin 18 is a Diagnostic and Prognostic Factor for Acute Alcoholic Hepatitis. Clin Gastroenterol Hepatol 2019;18:2046-2054.
51. Saha B, Tornai D, Kodys K, Adejumo A, Lowe P, McClain C, et al. Biomarkers of Macrophage Activation and Immune Danger Signals Predict Clinical Outcomes in Alcoholic Hepatitis. Hepatology 2019;70:1134-1149.
52. Cashman JR. Human flavin-containing monooxygenase (form 3): polymorphisms and variations in chemical metabolism. Pharmacogenomics 2002;3:325-339.
53. Craciun S, Balskus EP. Microbial conversion of choline to trimethylamine requires a glycyl radical enzyme. Proc Natl Acad Sci USA 2012;109:21307-21312.
54. Bantel H, Lugering A, Heidemann J, Volkmann X, Poremba C, Strassburg CP, et al. Detection of apoptotic caspase activation in sera from patients with chronic HCV infection is associated with fibrotic liver injury. Hepatology 2004;40:1078-1087.
55. Schugar RC, Willard B, Wang Z, Brown JM. Postprandial gut microbiota-driven choline metabolism links dietary cues to adipose tissue dysfunction. Adipocyte 2018;8:49-56.
56. Boutagy NE, Neilson AP, Osterberg KL, Smithson AT, Englund TR, Davy BM, et al. Short-term high-fat diet increases postprandial trimethylamine-N-oxide in humans. Nutr Res 2015;35:858-864.
57. Li Q, Korzan WJ, Ferrero DM, Chang RB, Roy DS, Buchi M, et al. Synchronous evolution of an odor biosynthesis pathway and behavioral response. Curr Biol 2013;23:11-20.
58. Wallrabenstein I, Kuklan J, Weber L, Zborala S, Werner M, Altmuller J, et al. Human trace amine-associated receptor TAAR5 can be activated by trimethylamine. PloS One 2013;8:e54950.

59. Chen S, Henderson A, Petriello MC, Romano KA, Gearing M, Miao J, et al. Trimethylamine N-oxide binds and activates PERK to promote metabolic dysfunction. Cell Metab 2019;30:1141-1151.

60. Huang LJ, Wang L, Ma Y, Durick K, Perkins G, Deerinck T, et al. NH2-terminal targeting motifs direct dual specificity A-kinase-anchoring protein 1 (D-AKAP1) to either mitochondria or endoplasmic reticulum. J Cell Biol 1999;145:951-959.

61. Nooh MM, Bahouth SW. Two barcodes encoded by the type-1 PDZ and by phosphor-ser312 regulate retromer/WASH-mediated sorting of the b1-adrenergic receptor from endosomes to the plasma membrane. Cell Signal 2017;29:192-208.

62. Araki E, Lipes MA, Patti ME, Bruning JC, Haag 3rd B, Johnson RS, Kahn CR. Alternative pathway of insulin signaling in mice with targeted disruption of the IRS-1 gene. Nature 1994;372:186-190.

63. Zhou W, Li X, Premont RT. Expanding functions of GIT Arf GTPase-activating proteins, PIX Rho guanine nucleotide exchange factors and GIT-PIX complexes. J Cell Sci 2016;129:1963-1974.

64. Asian JE. Platelet Rho GTPase regulation in physiology and disease. Platelets 2019;30:17-22.

65. Strub K, Walter P. Assembly of the Alu domain of the signal recognition particle (SRP): dimerization of the two protein components is required for efficient binding to SRP RNA. Mol Cell Biol 1990;10:777-784.

66. Cho S, Hoang A, Sinha R, Zhong X-Y, Fu X-D, Krainer AR, Ghosh G. Interaction between the RNA binding domains of Ser-Arg splicing factor 1 and U1-70K snRNP protein determines early spliceosome assembly. Proc Natl Acad Sci USA 2011;108:8233-8238.

67. Casaburi A, Piombino P, Nychas G-J, Villani F, Ercolini D. Bacterial populations and the volatilome associated to meat spoilage. Food Microbiol 2015;45:83-102.
68. Wortham BW, Patel CN, Oliveira MA. Polyamines in bacteria: pleiotropic effects yet specific mechanisms. Adv Exp Med Biol 2007;603:106-115.
69. Ihara S, Yoshikawa K, Touhara K. Chemosensory signals and their receptors in the olfactory neural system. Neuroscience 2013;254:45-60.
70. Zhang J, Chaluvadi MR, Reddy R, Motika MS, Richardson TA, Cashman JR, Morgan ET. Hepatic flavin-containing monooxygenase gene regulation in different mouse inflammation models. Drug Metab Dispos 2009;37:462-468.
71. Maier L, Pruteanu M, Kuhn M, Zeller G, Telzerow A, Anderson EE, et al. Extensive impact of non-antibiotic drugs on human gut bacteria. Nature 2018;555:623-628.
72. Wu H, Esteve E, Tremaroli V, Khan MT, Caesar R, Mannerås-Holm L, et al. Metformin alters the gut microbiome of individuals with treatment-naïve type 2 diabetes, contributing to the therapeutic effects of the drug. Nat Med 201723:850-858.
73. Bray NL, Pimentel H, Melsted P, Pachter L. Near-optimal probabilistic RNA-seq quantification. Nat Biotechnol 2016;34:525-527.
74. Pimentel H, Bray NL, Puente S, Melsted P, Pachter L. Differential analysis of RNA-seq incorporating quantification uncertainty. Nat Methods 2017;14:687-690.
75. Mistry JS, Abraham DJ, Kozikowski AP, Hanin I. Neurochemistry of Aging. 2. Design, Synthesis, and Biological Evaluation of Halomethyl Analogues of Choline with High Affinity Choline Transport Inhibitory Activity. J Med Chem 1991;34:2031-2036.
76. Bertola A, Matthews S, Ki SH, Wang B, Gao B. Mouse model of chronic and binge ethanol feeding (the NIAAA model). Nat Protoc 2013;8:627-637.
77. McMurdle PJ, Holmes S. Phyloseq: an R package for reproducible interactive analysis and graphics of microbiome census data. PloS one 2013;8:e61217.

78. Caporaso JG, Kuczunski J, Stombaugh J, Bittinger K, Bushman FD, Costello EK, et al. QIIME allows analysis of high-throughput community sequencing data. Nat Methods 2010;7:335-336.

79. Callahan BJ, McMurdie PJ, Rosen MJ, Han AW, Johnson AJA, Holmes SP. DADA2: high-resolution sample interference from illumine amplicon data. Nat Methods 2016;13:581-583.

80. Wickham H. ggplot2: Elegant graphics for data analysis (Springer Publishing Company, Incorporated, 2009).

81. Benjamini Y. Discovering the false discovery rate. Journal of the Royal Statistical Society: Series B (Statistical Methodology) 2010;72:405-416.

82. Tilt E-M. Nonparametric statistical methods. Myles Hollander and Douglas A. Wolfe, Wiley, Chichester, Statistics in Medicine 1999;19:1386-1388.

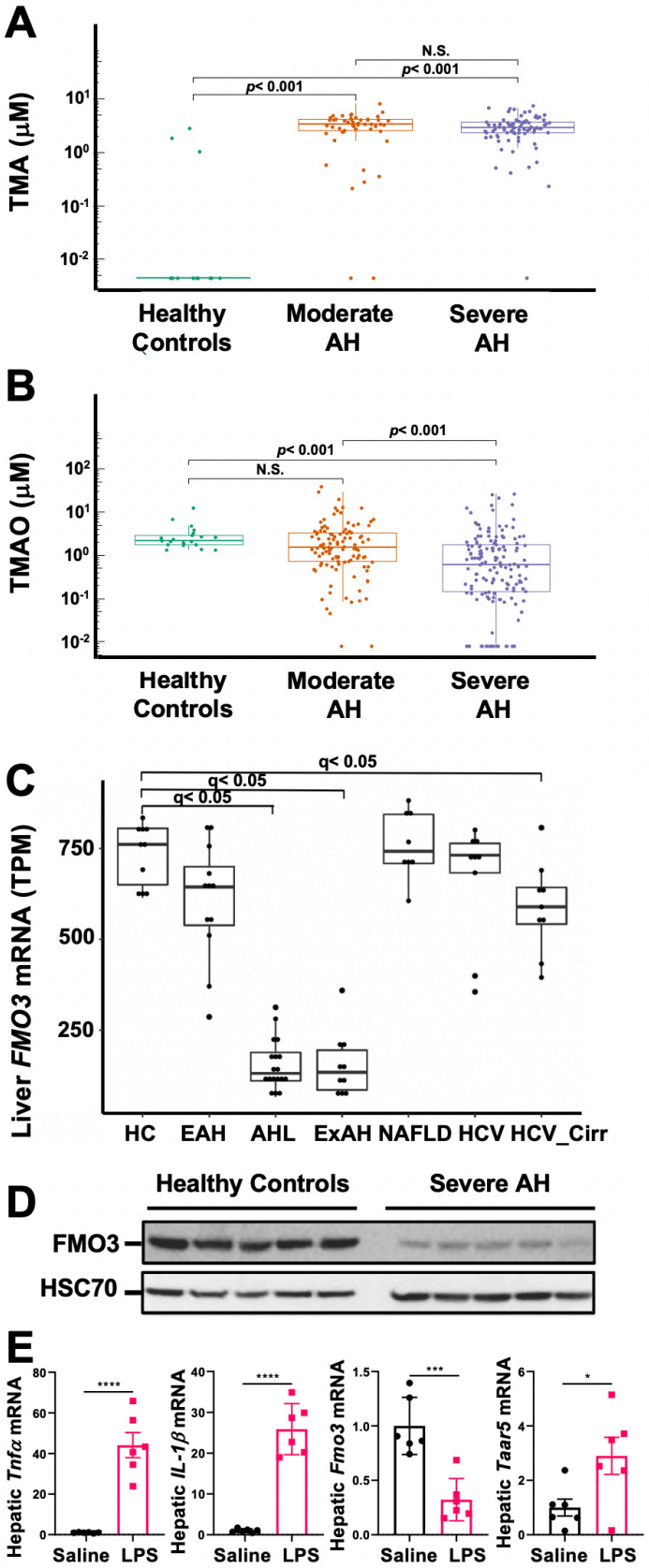

Figure 1. The Gut Microbial Volatile Metabolite Trimethylamine (TMA) is Elevated in Alcohol-Associated Hepatitis (AH). Plasma TMA *(A)* and TMAO *(B)* levels in patients

considered healthy (n-=13 for TMA and 20 for TMAO), or who have moderate (MELD<20) (n=52 for TMA and 111 for TMAO) or severe (MELD>20) (n=83 for TMA and 152 for TMAO) AH. *(C)* RNA-sequencing results from liver tissues of patients with different pathologies, including: healthy controls (HC, n = 10), early AH (EAH, n = 12; MELD 7-8), AH with liver failure (AHL, n = 18; MELD 22-28), explant tissue from patients with severe AH with emergency liver transplants (ExAH, n = 10; MELD 18-21), nonalcohol-associated fatty liver disease (NAFLD; n = 8), hepatitis C virus (HCV; n = 9), and hepatitis C virus with cirrhosis (HCV_Cirr, n = 9). Gene expression was measured by transcripts per million (TPM). Boxplots of average expression for *Fmo3* in different disease groups; error bars indicate SD (q <0.05 in comparison to healthy controls). *(D)* Liver FMO3 protein expression measured by Western Blot from healthy patients and patients with severe AH undergoing emergency liver transplant (Maddrey's discriminant function 45-187). *(E)* Liver *Tnfa, Il1b, Fmo3* and *Taar5* transcript levels were measured by QPCR from female WT mice injected with either saline or LPS for 6 hours. N=6; Unpaired student's t-test. *P≤0.05; ***P≤0.001

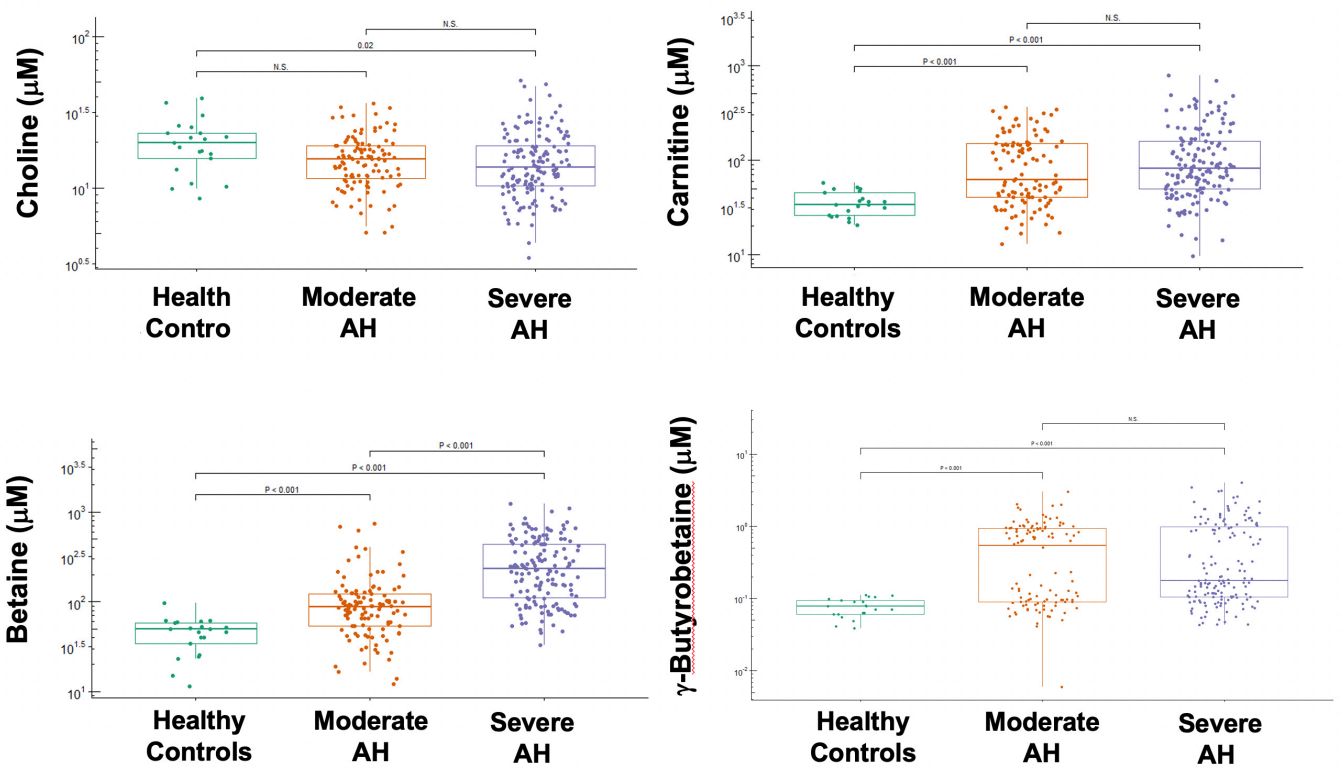

Figure 1-figure supplement 1: Levels of Trimethylamine (TMA)-Related Metabolites in Alcohol-Associated Hepatitis (AH). Boxplots depicting the plasma concentration of 4 trimethylamine (TMA)-related metabolites—choline, carnitine, betaine, and γ-butyrobetaine in healthy controls (n=21) and patients with moderate (n=112) and severe (n=152) alcoholic hepatitis (AH). Statistical significance was determined by analysis of variance and a Tukey's honest significant difference post-hoc test ($P < .05$).

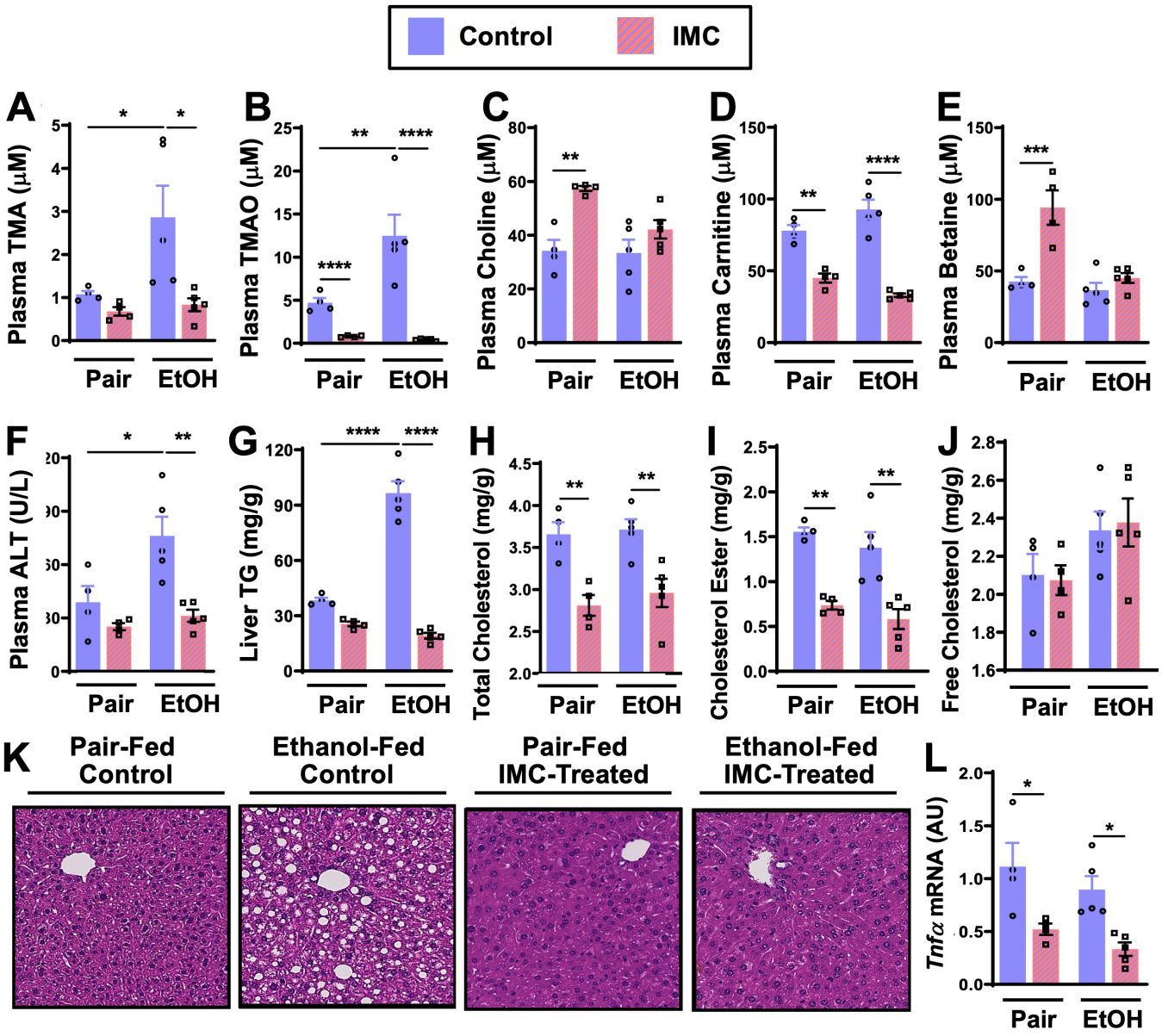

Figure 2. Small Molecule Choline TMA Lyase Inhibition with Iodomethylcholine (IMC) Protects Mice Against Ethanol-Induced Liver Injury. Nine to eleven week old female C57BL6/J mice were fed either ethanol-fed or pair-fed in the presence and absence of IMC as described in the methods. Plasma levels of TMA *(A)*, TMAO *(B)*, choline *(C)*, carnitine *(D)*, and betaine *(E)* were measured by mass spectrometry (n=4-5). Plasma alanine aminotransferase (ALT) *(F)* was measured enzymatically (n=4-5). Liver triglycerides *(G)*, total cholesterol *(H)*, cholesterol esters *(I)*, and free cholesterol *(J)* were measured enzymatically (n=4-5). *(K)* Representative H & E staining of livers from pair and EtOH-fed mice in the presence and

absence of IMC. *(L)* Hepatic messenger RNA levels of tumor necrosis factor alpha (*Tnf*α). Statistics were completed by a two-way ANOVA followed by a Tukey's multiple comparison test. **P*≤0.05; ***P*≤0.01; ****P*≤0.001; *****P*≤0.0001. All data are presented as mean ± S.E.M., unless otherwise noted.

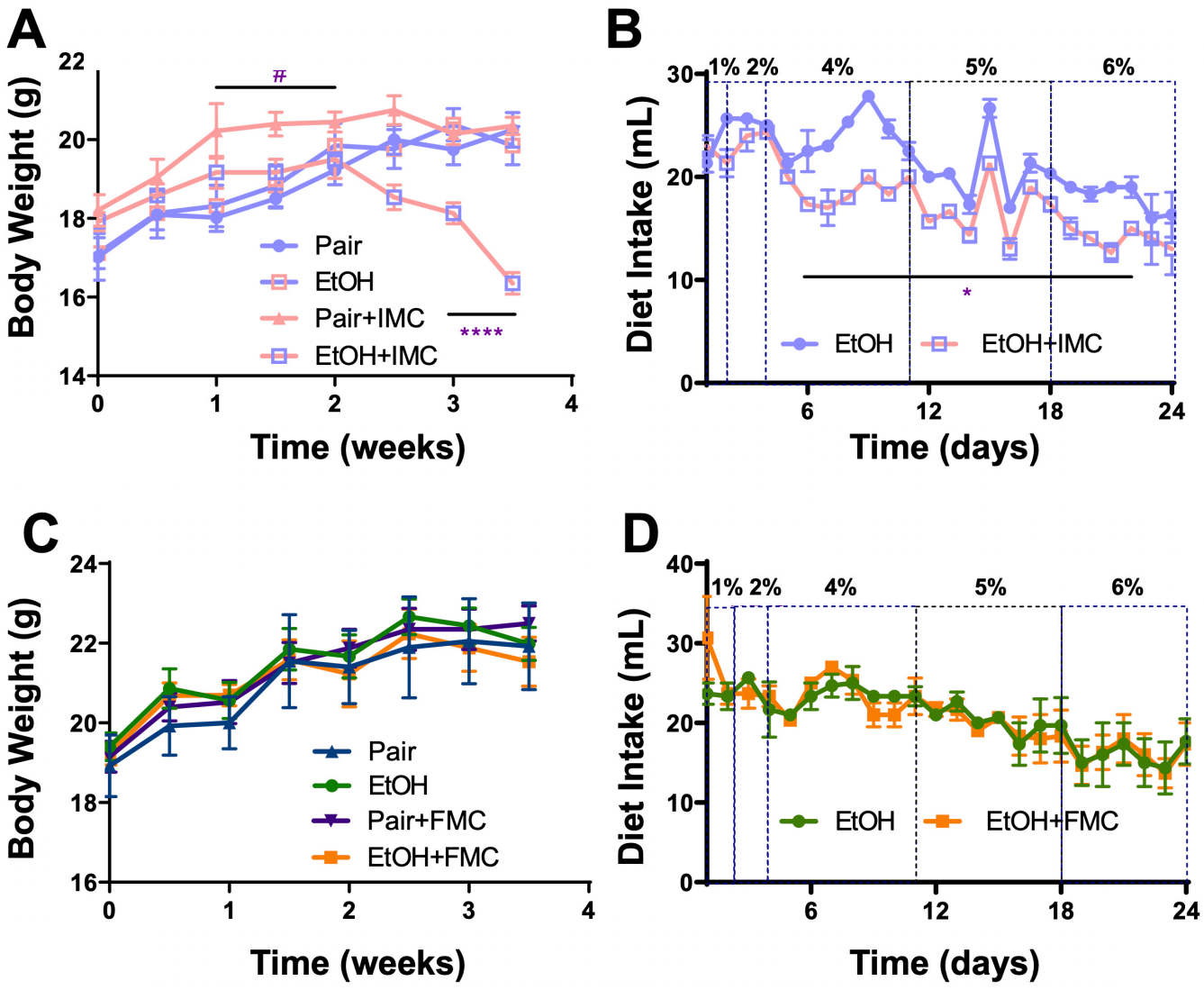

Figure 2-figure supplement 1. Small Molecule Inhibition with Iodomethylcholine (IMC), but not Fluoromethylcholine (FMC), Reduces Food Intake in Ethanol-Fed Mice. Panels A-B and C-D represent data from IMC and FMC-treated pair and ethanol-fed mice, respectively. (A, C) Body weights were measured biweekly throughout the 24-day experiment. #P≤0.05 comparing pair to pair+IMC; **** P≤0.0001 comparing ethanol to ethanol+IMC. (B, D) Diet intake was recorded daily throughout the experiment (n=3 cages of 6 mice per group). The ethanol percentages (1-6%) are listed on top of the figures. *P≤0.05 for days 6-22; n=4-6. Statistics were completed using a Student's t-test compared to the control mice. All data are presented as mean ± S.E.M., unless otherwise noted.

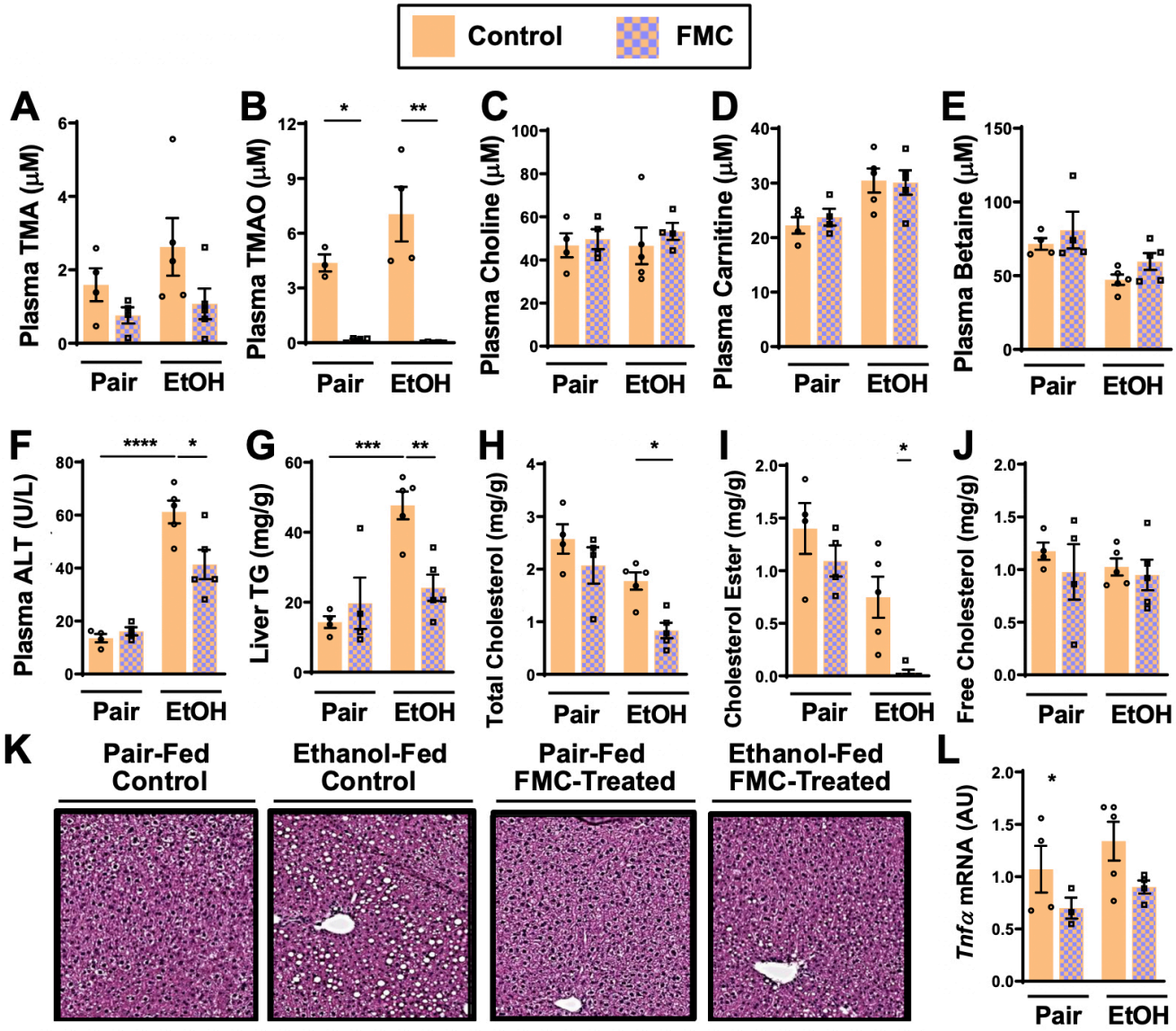

Figure 3. Small Molecule Choline TMA Lyase Inhibition with Fluoromethylcholine (FMC) Protects Mice Against Ethanol-Induced Liver Injury. Nine to eleven week old female C57BL6/J mice were fed either ethanol-fed or pair-fed in the presence and absence of FMC as described in the methods. Plasma levels of TMA *(A)*, TMAO *(B)*, choline *(C)*, carnitine *(D)*, and betaine *(E)* were measured by mass spectrometry (n=3-5). Plasma alanine aminotransferase (ALT) *(F)* were measured at necropsy (n=4-5). Liver triglycerides *(G)*, total cholesterol *(H)*, cholesterol esters *(I)*, and free cholesterol *(J)* were measured enzymatically (n=4-5). *(K)* Representative H & E staining of livers from pair and EtOH-fed mice in the presence and

absence of FMC. *(L)* Hepatic messenger RNA levels of tumor necrosis factor alpha (*Tnf*α). Statistics were completed by a two-way ANOVA followed by a Tukey's multiple comparison test. **P*≤0.05; ***P*≤0.01; ****P*≤0.001; *****P*≤0.0001. All data are presented as mean ± S.E.M., unless otherwise noted.

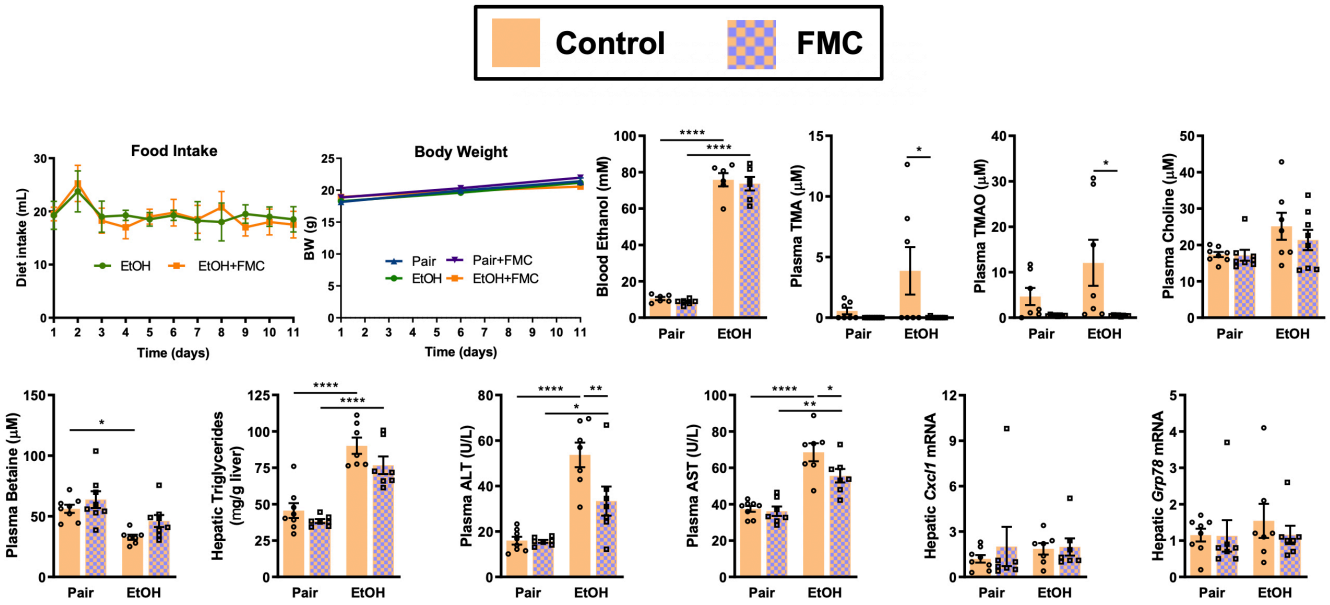

Figure 3-figure supplement 1. Small Molecule Inhibition of Gut Microbial TMA Lyase Activity with Fluoromethylcholine (FMC) in a Second Model of Ethanol-Induced Liver Injury. In this study, mice were exposed to a 10-day chronic model in which mice were allowed free access to a 5% vol/vol (27% kcal) for 10 days15. Ethanol-fed mice were allowed ad libitum access to liquid diet. Control mice were pair fed a diet that received isocalorically substituted maltose dextrin for ethanol. Some cohorts received choline TMA lyase inhibitor FMC (0.006% wt/wt) in these liquid diets throughout the entire 10-day feeding period. Statistics were completed by a two-way ANOVA followed by a Tukey's multiple comparison test. *P≤0.05; **P≤0.01; ***P≤0.001; ****P≤0.0001. All data are (n=5-8 per group) presented as mean ± S.E.M.

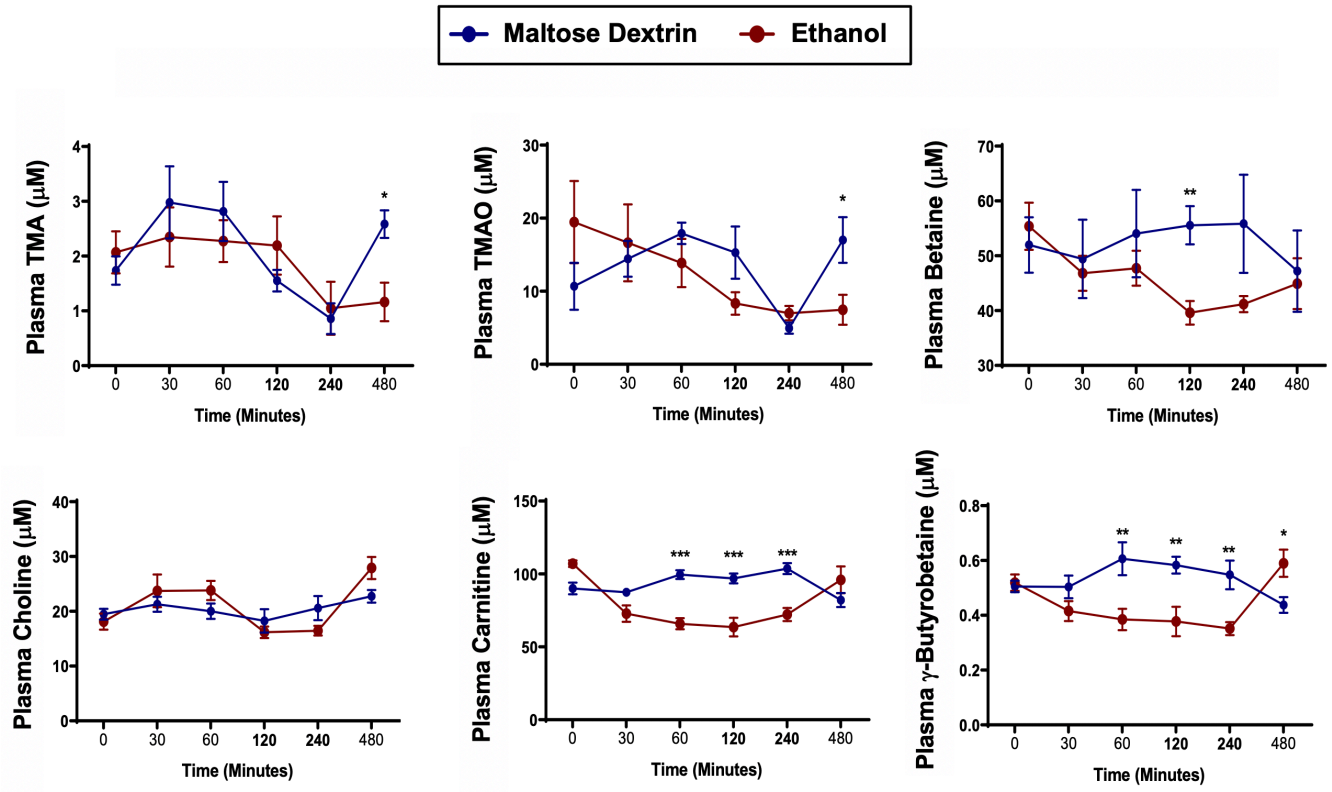

Figure 3-figure supplement 2. A Single Bolus of Ethanol Does Not Significantly Alter TMA or TMAO Levels in Mice. Nine to eleven week old female C57BL6/J mice were fed Lieber DeCarli liquid control diet for six days (n=5). On the seventh day, mice were gavaged with a bolus of maltose (9 g/kg) or ethanol (5 g/kg) and plasma was collected at several time points thereafter to examine acute alterations in trimethylamine (TMA) and related metabolites trimethylamine N-oxide (TMAO), betaine, choline, L-carnitine, and γ-butyrobetaine. Data were analyzed by a Student's t-test comparing the ethanol-fed mice to the maltose dextrin-gavaged mice. *P≤0.05; **P≤0.01; ***P≤0.001. All data are presented as mean ± S.E.M., unless otherwise noted.

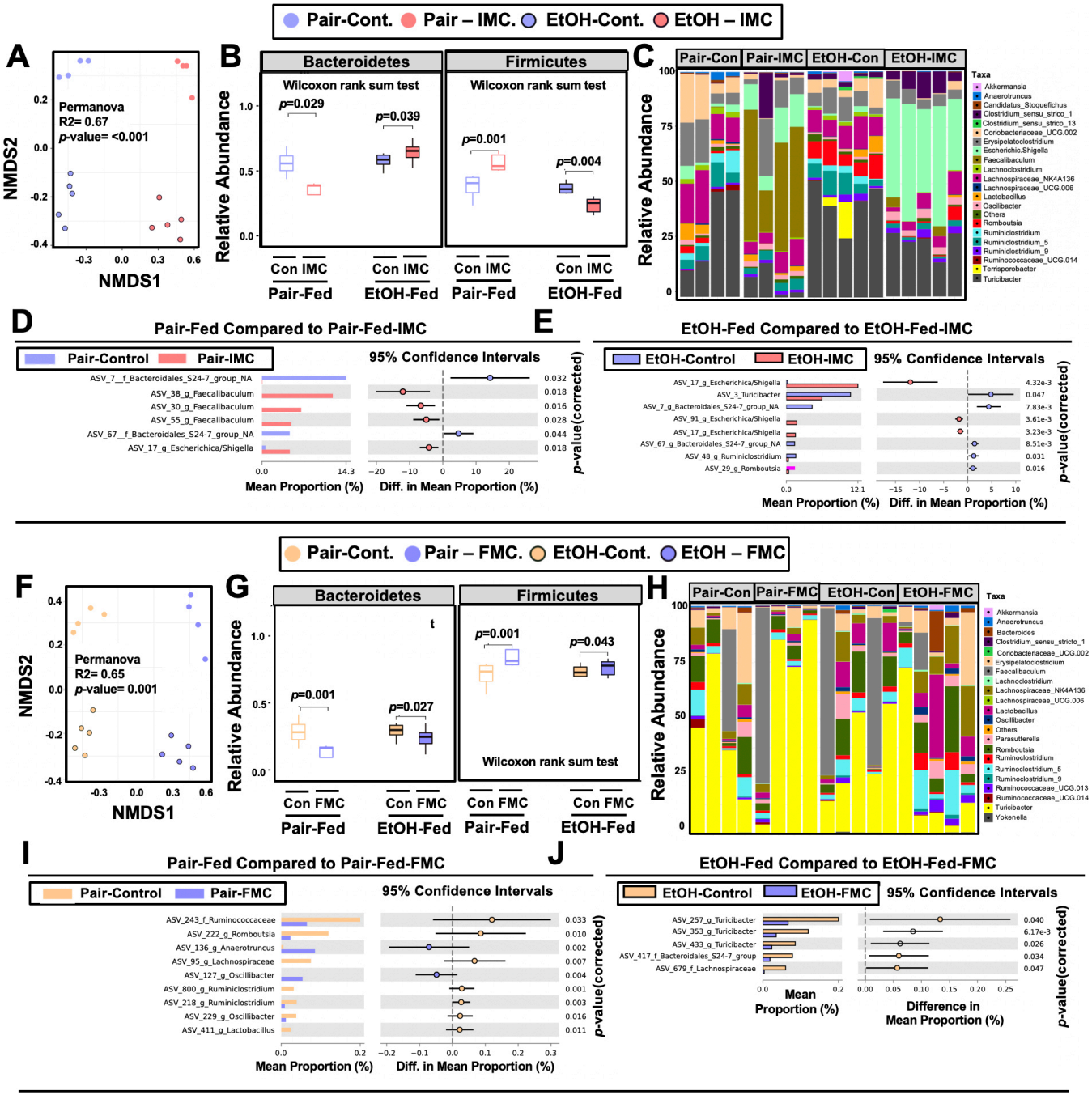

Figure 4. Small Molecule Choline TMA Lyase Inhibition Promotes Remodeling of the Gut Microbiome in an Ethanol-Dependent Manner. Nine to eleven week old female C57BL6/J mice were fed either ethanol-fed or pair-fed in the presence and absence of IMC or FMC as described in the methods. *(A)* NMDS plots based on the Bray-Curtis index between the Pair,

EtOH, Pair + 0.06% IMC and EtOH + 0.06% IMC groups, Statistical analysis was performed with PERMANOVA, and P values are labeled in plots. R^2 values are noted for comparisons with significant P values and stand for percentage variance explained by the variable of interest. *(B)* Box plots of relative abundance patterns for Firmicutes and Bacteroidetes distinguishing Pair, EtOH, Pair + 0.06% IMC and EtOH + 0.06% IMC groups. Statistical analysis was performed with Mann–Whitney U test (also called the *Wilcoxon rank-sum test*, p-values are labeled in plots). Plotted are interquartile ranges (boxes), and dark lines in boxes are medians. *(C)* Stacked bar charts of relative abundance (left y-axis) of the top 20 genera assembled across all four groups (Pair, EtOH, Pair + 0.06% IMC and EtOH + 0.06% IMC groups). Pairwise differential abundance analyses between *(D)* Pair-Fed and Pair-Fed + 0.06% IMC and *(E)* EtOH-Fed and EtOH-Fed + 0.06% IMC group. Statistical analysis was performed with White's non-parametric t-test (p-values are labeled in plots). *(F)* NMDS plots based on the Bray-Curtis index between the Pair, EtOH, Pair + 0.006% FMC and EtOH + 0.006% FMC groups, Statistical analysis was performed with PERMANOVA, and P values are labeled in plots. R^2 values are noted for comparisons with significant P values and stand for percentage variance explained by the variable of interest. *(G)* Box plots of relative abundance patterns for Firmicutes and Bacteroidetes distinguishing Pair, EtOH, Pair + 0.006% FMC and EtOH + 0.006% FMC groups. Statistical analysis was performed with Mann–Whitney U test (also called the *Wilcoxon rank-sum test*, p-values are labeled in plots). Plotted are interquartile ranges (boxes), and dark lines in boxes are medians. *(H)* Stacked bar charts of relative abundance (left y-axis) of the top 20 genera assembled across all four groups (Pair, EtOH, Pair + 0.06% FMC and EtOH + 0.006% FMC groups). Pairwise differential abundance analyses between *(I)* Pair-Fed and Pair-Fed + 0.06% FMC and *(J)* EtOH-Fed and EtOH-Fed + 0.006% FMC group. Statistical analysis was performed with White's non-parametric t-test (p-values are labeled in plots).

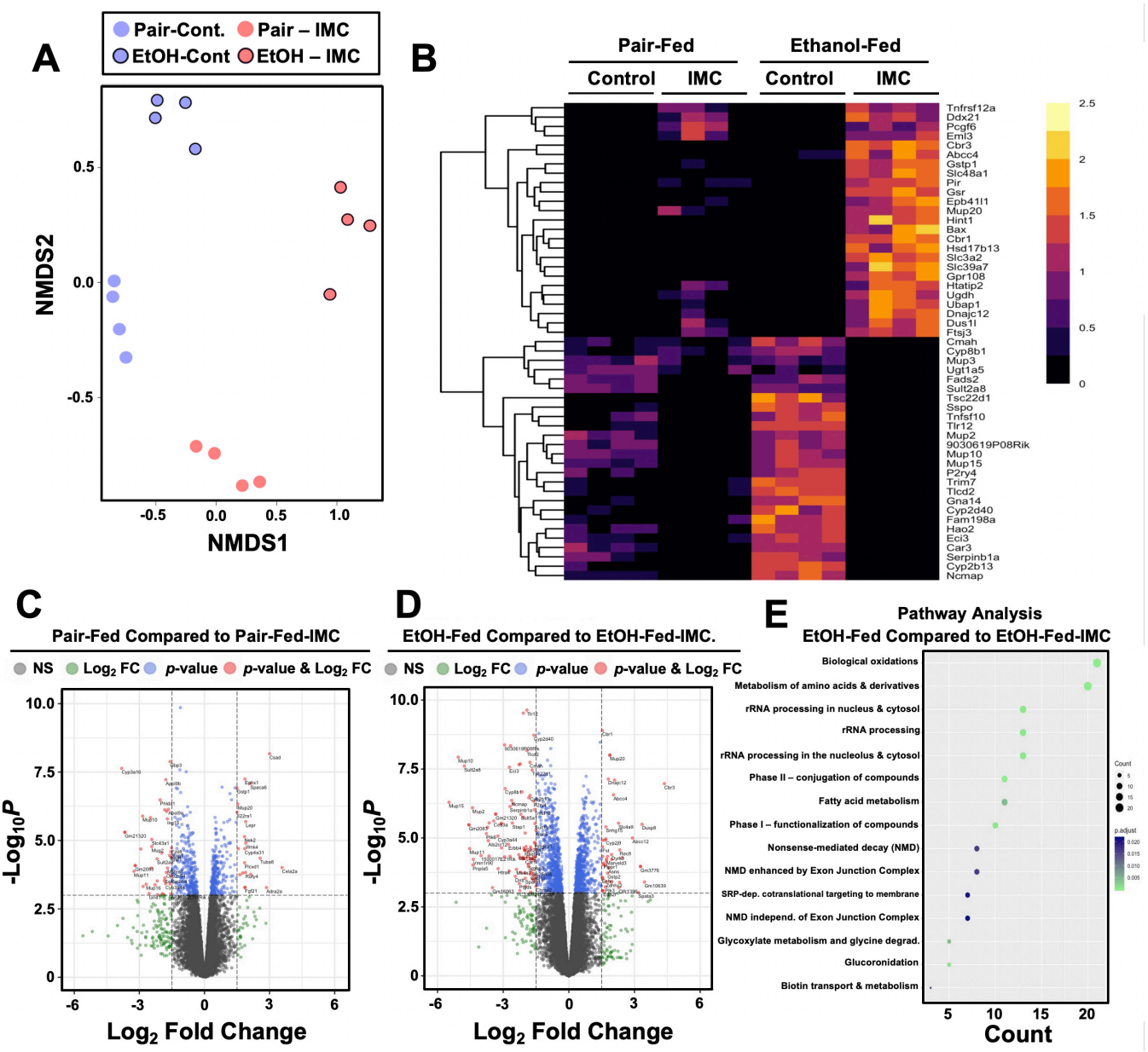

Figure 5. Small Molecule Choline TMA Lyase Inhibition with IMC Alters the Hepatic Transcriptome in Response to Ethanol. Nine to eleven week old female C57BL6/J mice were fed either ethanol-fed or pair-fed in the presence and absence of IMC as described in the methods. RNA was isolated from the livers and subjected to next generation sequencing. *(A)* NMDS Plots; Each point represents a single sample from a single mouse. Positions of points in space display dissimilarities in the transcriptome, with points further from one another being

more dissimilar. *(B-C)* Row-normalized expression for the top 25 DEGs shown by heat map *(B)* while the volcano plot *(C)* summarizes log2 fold changes vs significance in response to IMC treatment in pair (left) and ethanol (right) feeding (n=4). *(D)* Summary of significantly differentially regulated pathways in mice treated with IMC in the ethanol-fed mice (n=4).

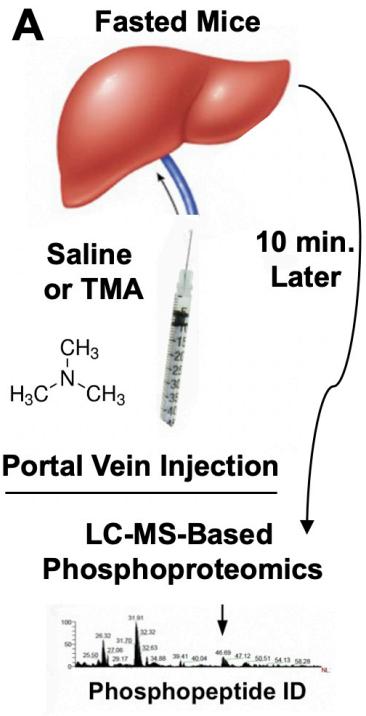

B **Phosphopeptides Altered by Portal TMA Injection**

Gene	Accesion	[M+H}	m/z	z	ΔM ppm	Sequence	TMA/Saline (*p*-value)
Arhgef6	Q8K4I3	1303.593	652.30115	2	1.57	KApSEEEYVIR.	0.27 (0.00096)
Akap1	O08715	2501.222	834.41205	3	-0.08	RLpSEEACPGVLSVAPTVTQPPGR	0.43 (0.00356)
Palmd	Q9JHU2	2146.805	716.27417	3	1.24	SGPQCSSPTCQEETEDVR + PO3	0.34 (0.00937)
Fkbp15	Q6P9Q6	1235.603	618.3056	2	0.64	RLpSLTPDPEK	0.29 (0.0105)
Srp14	P16254	1467.673	734.34064	2	0.9	KSpSVEGLEPAENK	3.64 (0.0114)
Hsp90ab1	P11499	2229.939	558.24115	4	1.48	EREKEIpSDDEAEEEKGEK	0.40 (0.0114)
Akap1	O08715	1499.637	750.32245	2	0.18	pSESSGNLPSVADTR	0.45 (0.0133)
Arhgap17	Q3UIA2	1302.573	651.79059	2	1.02	SSGTNFQGLPSK + PO3	0.28 (0.0141)
Nedd4l	Q8CFI0	1737.867	869.43774	2	0.68	SLpSSPTVTLSAPLEGAK	0.43 (0.0154)
Eif4g1	Q6NZJ6	1190.509	595.75867	2	0.96	pSFSKEVEER	2.74 (0.0166)
Irs2	P81122	1368.59	684.79987	2	1.54	RVpSGDGAQDLDR	0.45 (0.0182)
Hbs1l	Q69ZS7	1270.556	635.78198	2	0.34	SSQSESEIVPK + PO3	0.12 (0.0199)
F11r	O88792	1887.793	944.40216	2	2.38	VIYSQPpSTRpSEGEFK	0.30 (0.0207)
Washc2	Q6PGL7	1637.778	819.39404	2	1.59	VpSPEVGSADVASIAQK	0.45 (0.0232
Cyp2d11	P24457	1045.519	523.26379	2	1.23	RFpSVSTLR	0.37 (0.0236
Hdgf	P51859	2435.026	812.34814	3	1.49	GSAEGpSSDEEGKLVIDEPAKEK	2.36 (0.0249)
Wdr26	Q8C6G8	1397.642	699.32404	2	-0.9	RLpSQSDEDVIR	0.35 (0.0258)
Xrn2	Q9DBR1	2484.129	828.71539	3	1.06	NSSPSISPNTSFASDGSPSPLGGIK + PO3	0.36 (0.0262)
Clasp2	Q8BRT1	1454.664	727.83606	2	0.91	SRpSDIDVNAAAGAK	0.2 (0.0269)
Irf2bp2	E9Q1P8	1618.733	540.24933	3	0.07	RPApSVSSAAAEHEAR	0.37 (0.0277)
Srsf1	Q6PDM2	1577.687	789.34894	2	2.09	VKVDGPRpSPpSYGR	2.60 (0.0282)
Slc9a1	Q61165	968.4449	484.72601	2	-0.11	LDpSPTLSR	0.45 (0.0284)
Ei24	Q61070	1081.551	541.27942	2	0.16	RApSSLLAQR	0.48 (0.0304)
Pex1	Q5BL07	1856.748	928.87836	2	0.75	TPpSQEGCQDLTQEQR	0.37 (0.0318)
Zc3h4	Q6ZPZ3	1479.567	740.28833	2	1.94	TGTGpSPFAGNpSPAR	0.49 (0.0332)
Map3k20	Q9ESL4	1262.541	631.77533	2	1.67	SSSPTQYGLSR + PO3	0.23 (0.0354)
Tagln2	Q9WVA4	1359.558	680.28326	2	1.18	NFpSDNQLQEGK	0.35 (0.0371)
Ppp1r7	Q3UM45	2269.001	757.00592	3	0.98	HGGGGIVANLpSEQpSLKDGVDR	0.34 (0.0379)
Cdc42bpb	Q7TT50	2220.942	740.98584	3	0.52	HSTPSNSSNPSGPPpSPNSPHR	0.42 (0.0396)
Iws1	Q8C1D8	1780.667	890.84027	2	3.29	AAVLpSDpSEDDAGNASAK	0.25 (0.0397)
Nucb1	Q02819	1895.901	632.63977	3	1.92	SGKLpSQELDFVSHNVR	0.44 (0.0414)
Ttll12	Q3UDE2	1562.667	781.83698	2	-0.13	Ace-MEIQSGPQPGpSPGR	0.28 (0.0457)
Tnks1bp1	P58871	1010.467	505.73724	2	0.55	VSGAGLpSPSR	0.35 (0.0481)
Tgm1	Q9JLF6	1959.843	653.95313	3	0.75	RPEpSRGpSGVNAAGDGTIR	2.06 (0.0482)
Ccs	Q9WU84	1143.519	572.2641	2	1.32	KDpSAQPPAHL	0.42 (0.0494
Cyp2a5	P20852	1043.54	522.2738	2	0.55	RFpSIATLR	0.41 (0.0496)

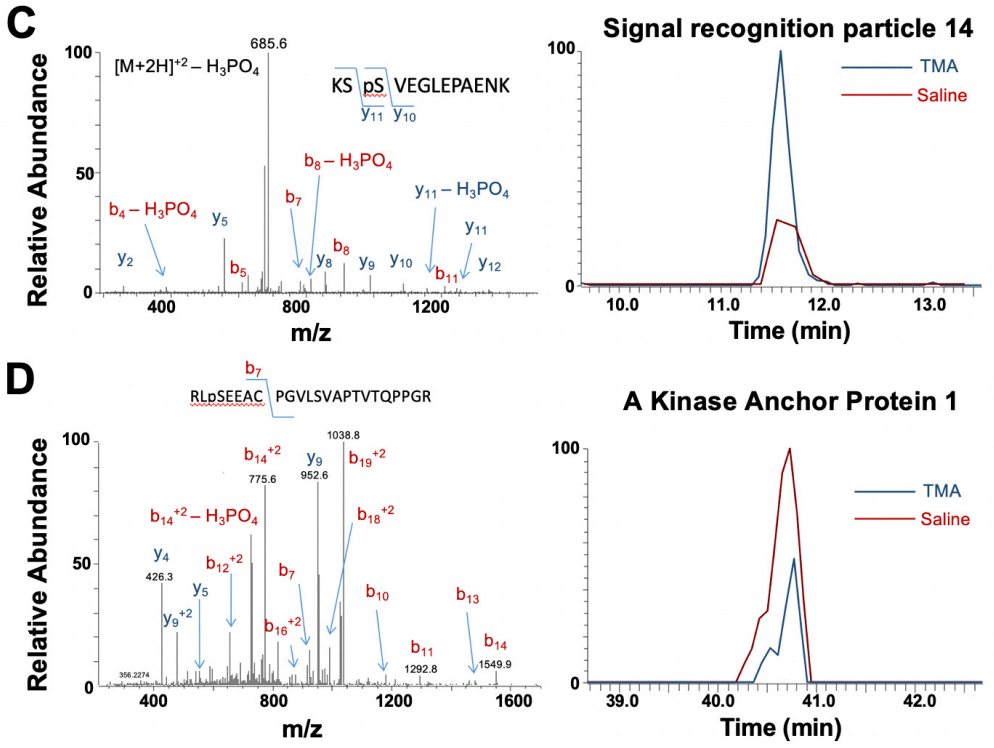

Figure 6. TMA Rapidly Reorganizes Liver Signal Transduction *In Vivo*. *(A)* Schematic of experiment; Female C57BL/6 mice were fasted overnight (12 hour fast), and then injected

directly into the portal vein with vehicle (saline), or TMA, and only 10 minutes later liver tissue was harvested for phosphoproteomic analysis to identify TMA-responsive phosphorylation events in mouse liver (n = 4 per group). *(B)* List of proteins that were differentially phosphorylated ($p<0.05$) upon TMA administration *in vivo*. *(C)* A doubly charged ion was present in the phospho-enriched sample that was identified as the KSpSVEGLEPAENK from Signal recognition particle 14 kDa protein (Srp14). The CID spectra of this ion is dominated by H_3PO_4 loss from the precursor ion consistent with the presence of a pS or pT residue. The mass difference between the y_{11} and y_{10} ions is consistent with modification at S45. The observed chromatograms for this peptide from the Saline and TMA samples is shown and the TMA/Saline ratio was determined to be 3.6 (p-value 0.0114). *(D)* A doubly charged ion was present in the phospho-enriched sample that was identified as the RLpSEEACPGVLSVAPTVTQPPGR from A-kinase anchor protein 1. The CID spectra of this ion is dominated by fragmentation C-terminal to the proline residues. The mass of the b_7 ion is consistent with modification at S55. The observed chromatograms for this peptide from the Saline and TMA samples is shown and the TMA/Saline ratio was determined to be 0.4.

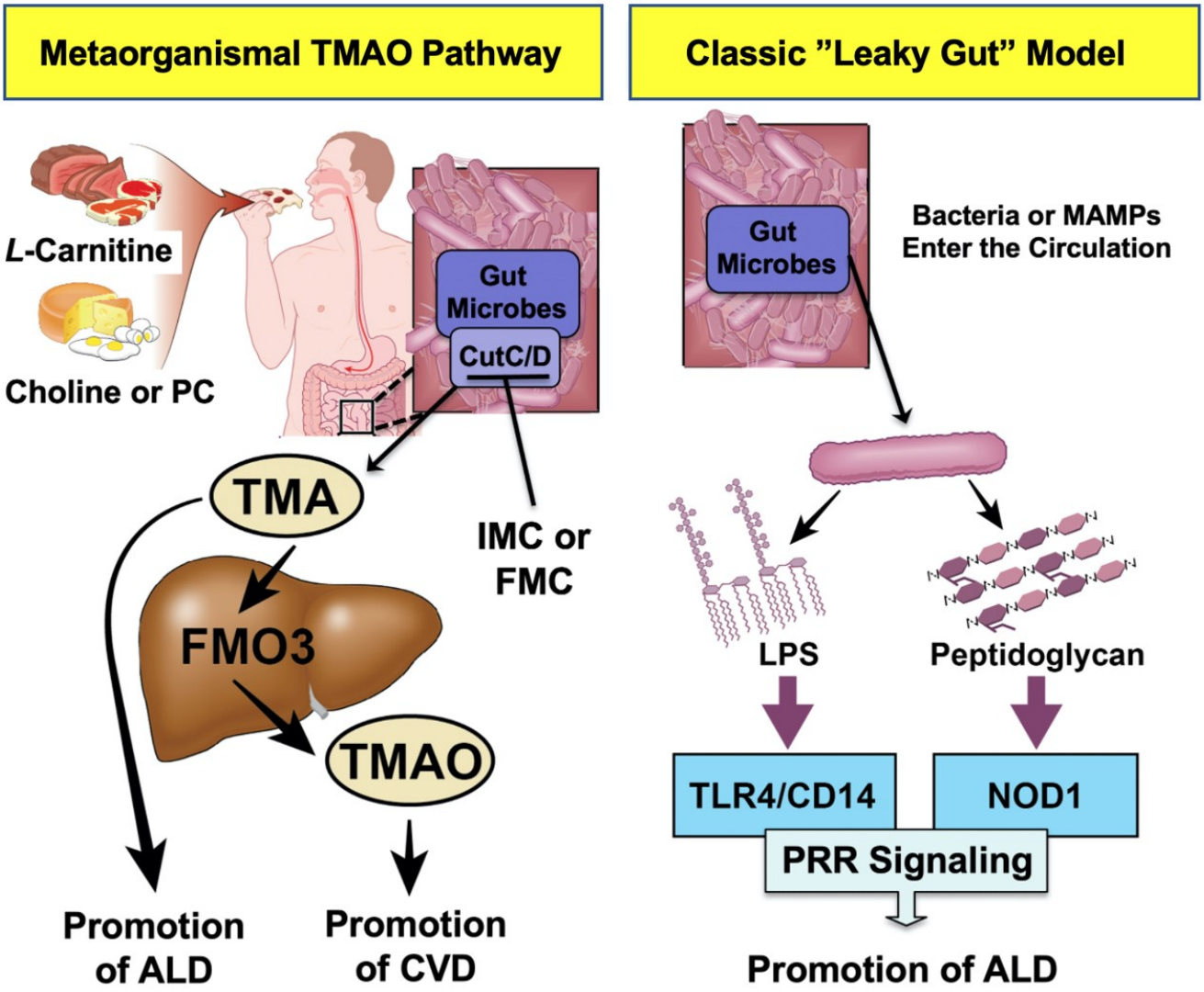

Figure 6-figure supplement 1. Graphical Summary Depicting the Proposed Role of TMA in the Progression of ALD. Gut microbiota can elicit both metabolism-dependent and metabolism-independent effects in ALD. Relevant to this manuscript, intestinal microbes metabolize dietary L-carnitine, choline, or phosphatidylcholine (PC) to form TMA, which is a volatile compound that originates exclusively from gut bacterial metabolism and is elevated in ALD. Importantly, TMA can also be converted to trimethylamine N-oxide (TMAO) by hepatic flavin monooxygenase 3 (FMO3), and TMAO has recently been linked to cardiovascular disease (CVD) promotion in humans. Metabolism-independent effects are the result of gut

hyperpermeability (leaky gut), allowing bacterial cell wall products such as lipopolysaccharide (LPS) and peptidoglycans to enter into the blood stream and engage with host pattern-recognition receptors (PRR) to promote hepatic inflammation. Collectively, metabolism-dependent pathways such as TMA production as well as metabolism independent pathways provide multiple bacterially-derived “hits” to promote ALD progression. The small molecule bacterially-targeted CutC/D inhibitors iodomethylcholine (IMC) and fluoromethylcholine (FMC) can effectively blunt ethanol-induced liver injury in mice.

Figure 1-table supplement 1: Demographic and clinical parameters for entire cohort of healthy controls and patients with AH (including DASH and NOAC biorepository enrollees).

	Healthy Control (N=21)	Alcohol Hepatitis Moderate (N=112)	Alcohol Hepatitis Severe (N=152)	Total (N=285)
Race (N, %)				
African American	0 (0.0%)	6 (5.4%)	12 (7.9%)	18 (6.3%)
Asian	1 (4.8%)	1 (0.9%)	0 (0.0%)	2 (0.7%)
Other	0 (0.0%)	1 (0.9%)	1 (0.7%)	2 (0.7%)
White	20 (95.2%)	104 (92.9%)	139 (91.4%)	263 (92.3%)
Gender (N, %)				
Female	12 (57.1%)	48 (42.9%)	62 (40.8%)	122 (42.8%)
Age (years)				
Median	42	49.5	48	49
Mean (SE)	43.09 (3.18)	48.42 (1.06)	46.37 (0.8)	46.937 (0.64)
Site (N, %)				
CCF	21 (100%)	28 (25.0%)	48 (31.6%)	97 (34.0%)
Louisville	0 (0.0%)	9 (8.0%)	13 (8.6%)	22 (7.7%)
UMMS	0 (0.0%)	49 (43.8%)	35 (23.0%)	84 (29.5%)
UTSW	0 (0.0%)	26 (23.2%)	56 (36.8%)	82 (28.8%)
AUDIT Score†				
Median	ND	25	25	25
Mean (SE)	ND	22.03 (1.61)	23.03 (1.07)	22.70 (0.88)
Laboratory Results				
Bilirubin (mg/dL)				
Median	ND	3.30	17.35	11.60
Mean (SE)	ND	5.06 (0.52)	18.87 (0.74)	13.06 (0.64)
AST (U/L)				
Median	ND	78	110.5	99
Mean (SE)	ND	99.66 (7.09)	131.13 (10.24)	117.88 (6.70)
ALT (U/L)				
Median	ND	34	40.5	39
Mean (SE)	ND	45.42 (3.51)	49.11 (3.03)	47.56 (2.29)
INR††				

Median	ND	1.2	1.8	1.6
Mean (SE)	ND	1.29 (0.03)	1.912 (0.04)	1.65 (0.03)
Creatinine (mg/dL)				
Median	ND	0.71	0.79	0.75
Mean (SE)	ND	0.75 (0.03)	1.11 (0.08)	0.96 (0.05)
Albumin (g/dL)				
Median	ND	3.10	2.60	2.70
Mean (SE)	ND	3.22 (0.07)	2.64 (0.04)	2.88 (0.04)
Alkaline phosphatase (U/L)				
Median	ND	130.00	153.50	146.00
Mean (SE)	ND	150.89 (8.38)	178.543 (8.734)	166.59 (6.19)
White blood cells (10^3/mm^3)				
Median	ND	6.20	9.34	8.14
Mean (SE)	ND	7.27 (0.37)	11.68 (0.58)	9.82 (0.40)
Total Protein (g/dL)				
Median	ND	6.70	6.00	6.30
Mean (SE)	ND	6.68 (0.11)	5.96 (0.07)	6.27 (0.07)
Prognostic Scores				
MELD Score§				
Median	ND	14	25	22
Mean (SE)	ND	13.50 (0.42)	25.96 (0.41)	20.76 (0.48)
Child-Turcotte Pugh Score¶				
Median	ND	8	10	10
Mean (SE)	ND	7.81 (0.11)	10.53 (0.11)	9.36 (0.13)
Maddrey's Discriminant Function‡				
Median	ND	12.30	52.64	35.11
Mean (SE)	ND	12.32 (1.30)	56.80 (2.14)	37.63 (1.94)

† AUDIT Questionnaire = Alcohol Use Disorders Identification Test
†† INR: international normalized ratio (*INR*) is a calculation based on results of a Prothrombin Time

§ In the Model for End-Stage Liver Disease (MELD), scores range from 6 to 40, with higher scores indicating worse prognosis.

¶ Child-Turcotte-Pugh Score classes for cirrhosis severity: A = 5-6 points; B = 7-9 points; C = 10-15 points

‡ Maddrey's Discriminant function is calculated as 4.6 × (patient's prothrombin time in seconds − lab control's prothrombin time in seconds) + patient's serum bilirubin level in milligrams per deciliter; a value of 32 or higher indicates severe alcoholic hepatitis that carries an adverse prognosis.

Figure 1-table supplement 2: Demographic and clinical parameters for subset of healthy controls and patients with AH (including DASH and NOAC biorepository enrollees) included in TMA assay.

	Healthy Control (N=13)	Alcohol Hepatitis Moderate (N=52)	Alcohol Hepatitis Severe (N=83)	Total (N=148)
Race (N, %)				
African American	0 (0.0%)	3 (5.8%)	5 (6.0%)	8 (5.4%)
Asian	1 (7.7%)	0 (0.0%)	0 (0.0%)	1 (0.7%)
Other	0 (0.0%)	1 (1.9%)	0 (0.0%)	1 (0.7%)
White	12 (92.3%)	48 (92.3%)	78 (94.0%)	138 (93.2%)
Gender (N, %)				
Female	7 (53.8%)	24 (42.3%)	33 (39.8%)	62 (41.9%)
Age (years)				
Median	42	49	47	48
Mean (SE)	41.4 (4.2)	47.46 (1.75)	45.96 (1.04)	46.08 (0.87)
Site (N, %)				
CCF	13 (100%)	12 (23.1%)	15 (18.1%)	40 (27.0%)
Louisville	0 (0.0%)	0 (0.0%)	0 (0.0%)	0 (0.0%)
UMMS	0 (0.0%)	21 (40.4%)	28 (33.7%)	49 (33.1%)
UTSW	0 (0.0%)	19 (36.5%)	40 (48.2%)	59 (39.9%)
AUDIT Score†				
Median	ND	23	24	24
Mean (SE)	ND	19.86 (2.35)	22.22 (1.66)	21.42 (1.35)
Laboratory Results				
Bilirubin (mg/dL)				
Median	ND	4.10	16	11.50
Mean (SE)	ND	4.49 (0.52)	18.18 (1.01)	12.99 (0.88)
AST (U/L)				
Median	ND	78	99	93
Mean (SE)	ND	99.42 (10.45)	118.15 (8.06)	111.00 (6.41)
ALT (U/L)				
Median	ND	31	45	38

Mean (SE)	ND	43.98 (5.09)	49.23 (4.22)	47.23 (3.25)
INR††				
Median	ND	1.25	1.90	1.60
Mean (SE)	ND	1.34 (0.05)	1.97 (0.06)	1.74 (0.05)
Creatinine (mg/dL)				
Median	ND	0.71	0.81	0.77
Mean (SE)	ND	0.766 (0.04)	1.04 (0.11)	0.94 (0.07)
Albumin (g/dL)				
Median	ND	3.30	2.60	2.70
Mean (SE)	ND	3.26 (0.11)	2.70 (0.06)	2.92 (0.06)
Alkaline phosphatase (U/L)				
Median	ND	128.00	147.00	140.50
Mean (SE)	ND	140.37 (10.42)	170.74 (10.24)	159.29 (7.58)
White blood cells ($10^3/mm^3$)				
Median	ND	6.00	8.86	7.60
Mean (SE)	ND	7.29 (0.53)	10.75 (0.73)	9.51 (0.53)
Total Protein (g/dL)				
Median	ND	6.70	6.00	6.20
Mean (SE)	ND	6.65 (0.16)	6.02 (0.10)	6.25 (0.09)
Prognostic Scores				
MELD Score§ Median Mean (SE)	ND ND	16 14.08 (0.66)	25 25.54 (0.56)	22 21.28 (0.65)
Child-Turcotte Pugh Score¶ Median Mean (SE)	ND ND	8 8.043 (0.26)	10 10.41 (0.13)	10 9.53 (0.16)
Maddrey's Discriminant Function‡ Median Mean (SE)	ND ND	14.42 13.50 (1.79)	51.88 56.54 (2.88)	36.57 40.56 (2.64)

† AUDIT Questionnaire = Alcohol Use Disorders Identification Test

†† INR: international normalized ratio (*INR*) is a calculation based on results of a Prothrombin Time

§ In the Model for End-Stage Liver Disease (MELD), scores range from 6 to 40, with higher scores indicating worse prognosis.

¶ Child-Turcotte-Pugh Score classes for cirrhosis severity: A = 5-6 points; B = 7-9 points; C = 10-15 points

‡ Maddrey's Discriminant function is calculated as 4.6 × (patient's prothrombin time in seconds − lab control's prothrombin time in seconds) + patient's serum bilirubin level in milligrams per deciliter; a value of 32 or higher indicates severe alcoholic hepatitis that carries an adverse prognosis.